AGU PUBLICATIONS

Geochemistry, Geophysics, Geosystems

RESEARCH ARTICLE

10.1002/2017GC007089

Special Section:
Clumped Isotope Geochemistry: From Theory to Applications

Near Equilibrium $^{13}C—^{18}O$ Bonding During Inorganic Calcite Precipitation Under Chemo-Stat Conditions

Nicholas P. Levitt[1], John M. Eiler[2], Christopher S. Romanek[3], Brian L. Beard[1], Huifang Xu[1], and Clark M. Johnson[1]

[1]NASA Astrobiology Institute and Department of Geoscience, University of Wisconsin-Madison, Madison, Wisconsin, USA, [2]NASA Astrobiology Institute and Geological and Planetary Sciences, California Institute of Technology, Pasadena, California, USA, [3]NASA Astrobiology Institute and Department of Earth and Environmental Sciences, Furman University, Greenville, South Carolina, USA

Key Points:
- We report results of C, O, and "clumped" isotope analyses from chemo-stat calcite precipitation experiments under laboratory conditions
- An inverse relation between saturation state (SS) and clumping is observed, where high SS is furthest from equilibrium $^{13}C—^{18}O$ partitioning
- Carbonate growth approached equilibrium more closely than previous experiments of this type, yet did not achieve full O isotope equilibrium

Supporting Information:
- Supporting Information S1

Correspondence to:
N. P. Levitt,
nlevitt@wisc.edu

Citation:
Levitt, N. P., Eiler, J. M., Romanek, C. S., Beard, B. L., Xu, H., & Johnson, C. M. (2018). Near equilibrium $^{13}C—^{18}O$ bonding during inorganic calcite precipitation under chemo-stat conditions. *Geochemistry, Geophysics, Geosystems*, *19*, 901–920. https://doi.org/10.1002/2017GC007089

Received 28 JUN 2017
Accepted 13 FEB 2018
Accepted article online 26 FEB 2018
Published online 23 MAR 2018
Corrected 9 APR 2018

This article was corrected on 9 APR 2018. See the end of the full text for details.

Abstract We report results of $^{13}C/^{12}C$, $^{18}O/^{16}O$, and $^{13}C—^{18}O$ "clumped" isotope analyses from a series of calcite precipitation experiments from aqueous solutions under laboratory conditions. Chemo-stat precipitation experiments were performed to synthetically form calcite from aqueous solution onto ^{43}Ca-labeled calcite seed crystals. Formation rate was controlled during the experiments to investigate the effect of precipitation rate and temperature on $^{13}C—^{18}O$ bonding in calcite, where rates ranged from $10^{-6.88}$ to $10^{-8.20}$ mol m^{-2} s^{-1} at three temperatures (10, 20, and 30°C). No relation was observed between precipitation rate and $^{13}C—^{18}O$ bonding proportion over the range of precipitation rates used. The relation between Δ_{47} and temperature produced was comparable to calibration studies which report a relatively high sensitivity of $^{13}C—^{18}O$ bonding to temperature over the range investigated. Comparing solution conditions across multiple experimental data sets indicates an inverse relation between saturation state and $^{13}C—^{18}O$ bonding, where high super-saturation conditions are likely to be furthest from equilibrium $^{13}C—^{18}O$ partitioning. Carbon fractionation between calcite and $HCO_{3(aq)}^{-}$ was found to be a temperature independent value of $+1.6‰$. The temperature-dependent calcite-water $^{18}O/^{16}O$ fractionation relation determined in this study is slightly different (larger $\alpha_{calcite\text{-}H_2O}$ value) than those measured in several previous investigations. Significantly, we observe a dependence of the $^{18}O/^{16}O$ isotope fractionation factor on growth rate. Taken together, these findings suggest carbonate growth in our experiments approached equilibrium more closely than previous experiments of this type, yet did not achieve full O isotope equilibrium.

1. Introduction

Oxygen isotope thermometry has a long and important history in geoscience, where, for example, $^{18}O/^{16}O$ fractionation between carbonate and water has been extensively applied as a paleothermometer (Epstein et al., 1953; McCrea, 1950; Urey, 1947). Application of the O isotope carbonate paleothermometer, however, has been hindered by the large range in temperature-dependent carbonate-water fractionations observed in experimental and empirical studies, such that there is currently no consensus on the correct equilibrium carbonate-water $^{18}O/^{16}O$ fractionation curve (Coplen, 2007; Kim & O'Neil, 1997; Mills & Urey, 1940; O'Neil & Adami, 1969; Watkins & Hunt, 2015; Zeebe, 2014). Recently, a stable isotope thermometer has been proposed involving multiply substituted, or "clumped," isotopologues of carbonate, which has the potential advantage that temperature can be constrained through measurements of carbonate alone, without knowledge of the O isotope composition of the water from which carbonate grew (Dennis & Schrag, 2010; Eiler, 2007; Ghosh et al., 2006; Wang et al., 2004). In addition, clumped isotope analysis allows calculation of the isotopic composition of formation fluid (Eiler, 2011). This technique has been used to investigate the temperatures of deposition and $\delta^{18}O$ of seawater based on measurements of marine carbonates throughout the Phanerozoic, addressing longstanding debates as to whether variations in $\delta^{18}O$ of marine carbonates reflect changes in temperature or seawater O isotope compositions, and in some cases clarifying the role of diagenesis in stable isotope compositions of ancient carbonates (Came et al., 2007; Cummins et al., 2014; Finnegan et al., 2011).

The study of clumped isotopes involves quantification of the preferential bonding between rare stable isotopes (^{13}C to ^{18}O in carbonates) in multiply substituted isotopologues as compared to that predicted from

stochastic arrangement. In systems that achieve or closely approach thermodynamic equilibrium, the abundances of multiply substituted isotopologues are controlled by the effects of isotopic substitution on the reduced masses, and therefore vibration frequencies of the fundamental modes of molecular vibration (and/or rotation). Singly substituted species generally have lower vibration frequencies than their isotopically "normal" (isotopes of highest abundance) equivalents, and therefore are energetically favored. The doubly substituted species have their vibrational frequencies lowered even more—importantly, usually by slightly more than twice the energy benefit of a single substitution. For that reason, it is energetically favorable to organize the rare heavy isotopes into bonds with each other, where the reduction in system energy is greatest. This energetic effect is counter-acted by configurational entropy, which promotes random distribution of isotopes among all possible isotopologues. In turn, this entropy would produce isotopic ratios that scale with relative atomic abundances and is increasingly important with increasing temperature. It is the balance between the bond-vibration effect and the configurational entropy effect that leads to the temperature dependence of clumped isotope reactions (Eiler, 2007; Urey, 1947; Wang et al., 2004).

The first empirical clumped isotope thermometry calibration for calcite was determined by Ghosh et al. (2006) using synthetic calcite, and confirmed using natural calcium carbonate precipitated from surface and deep-sea corals that grew at known temperatures. Subsequently, several other calibration studies have been conducted to explore $^{13}C—^{18}O$ bonding during carbonate precipitation (Bonifacie et al., 2017, and references therein; Kelson et al., 2017; Tang et al., 2014; Tripati et al., 2015; Zaarur et al., 2013). With the proliferation of laboratories performing such measurements and calibrations of increasingly diverse materials, it has become clear that there are discrepancies among some calibrations of temperature-dependent carbonate clumped isotope compositions. At least some such discrepancies appear to reflect interlaboratory biases rather than material-specific properties of the carbonates themselves (although there is no consensus as of yet as to exactly why this is so). It is also recognized that some component of variations in carbonate clumped isotope calibrations can reflect differences in thermodynamically controlled equilibrium constants for different forms of carbonate (HCO_3^- versus CO_3^{2-}; calcite versus aragonite; Hill et al., 2014; Schauble et al., 2006; Tripati et al., 2015) or possibly even different acid digestion fractionation factors between calcite and aragonite (Guo et al., 2009).

Some component of these discrepancies, however, likely also reflects different extents of kinetically controlled isotopic fractionation during growth of calibration minerals. It has long been recognized that kinetic effects, and variations in the approach to equilibrium, are likely factors in discrepancies between calibrations of the carbonate-water $^{18}O/^{16}O$ thermometer (Gabitov et al., 2012, Sade & Halevy, 2017; Watkins et al., 2014). By extension, it seems plausible that the same is true of the carbonate clumped isotope thermometer. Such kinetic effects can reflect any of several factors: transport (such as by diffusion); unidirectional hydration, hydroxylation, dehydration or dehydroxilation; solid mineral precipitation rates (Kluge et al., 2014; Tang et al., 2014; Tripati et al., 2015; Watkins & Hunt, 2015); and enzymatic or "vital effects" (Came et al., 2014; Eagle et al., 2013; Petryshyn et al., 2015; Tripati et al., 2010). On short time scales, CO_2 dissolution and degassing have been shown to disrupt clumped isotope equilibrium in the dissolved inorganic C (DIC) pool (Affek et al., 2014; Affek & Zaarur, 2014). However, worth distinguishing is the difference between disequilibrium in the DIC pool related to systems such as speleothems (Daeron et al., 2011; Kluge & Affek, 2012; Kluge et al., 2013) and coral vital effects (Saenger et al., 2012; Spooner et al., 2016) compared to the effect of precipitation rates and mineral surface dynamics that may be partially or fully decoupled from the solution DIC pool (see section 4). This body of evidence suggests that additional experimental work focusing on alternative precipitation regimes may provide further understanding of equilibrium versus kinetic processes during carbonate precipitation.

In this study, we systematically assess precipitation rate as a variable in determining equilibrium versus kinetic stable isotope fractionations during synthetic carbonate mineral formation, both in terms of bulk $^{13}C/^{12}C$ and $^{18}O/^{16}O$ fractionations, as well as carbonate clumped ($^{13}C—^{18}O$) isotope compositions. Most previous experimental work has used CO_2 degassing, diffusion, and/or the manipulation of *p*H to promote carbonate precipitation. For clumped isotope thermometry, such approaches risk producing a DIC pool that is shifted away from clumped and O isotope equilibrium (Affek, 2013) over the course of precipitation. Our approach used constant solution chemical and isotopic compositions ("chemo-stat") to avoid transient changes in clumped isotope composition of the DIC pool. In addition, a unique aspect of this study is our use of seed crystals to remove the potential complicating factor of isotope fractionation attributed to

homogeneous nucleation mechanisms and/or high initial precipitation rate (Gabitov et al., 2012; Romanek et al., 2011). This approach allowed us to avoid potential CO_2 degassing effects. In addition, we were able to obtain carbonate precipitation using solution compositions that were only slightly supersaturated with respect to calcite (one to four times equilibrium saturation, i.e., $\Omega = 1–4$), a much lower level relative to previous studies, which report up to 525 times supersaturation (Dennis & Schrag, 2010; Kelson et al., 2017; Tang et al., 2014). Experiments were conducted over a temperature range of 10–30°C and a range of precipitation rates from 0.006 to 0.132 μmol m^{-2} s^{-1}, significantly slower than those of most previous studies, where documented growth rates were as high as 5.939 μmol m^{-2} s^{-1} (Dietzel et al., 2009; Tang et al., 2014). The results of our study show that carbonate growth with these methods, and including the slow rates of precipitation, yields carbonate clumped isotope compositions that are essentially independent of growth rate, and consistent with a subset of previous calibrations (esp., Ghosh et al., 2006, Zaarur et al., 2013, and calibrations of similar slope produced in those two labs).

2. Materials and Methods

This study employed the carbonate precipitation approach commonly referred to as a "chemo-stat" technique (Jimenez-Lopez & Romanek, 2004; Morse, 1974; Mucci & Morse, 1983; Romanek et al., 1992). Conditions were monitored during each experiment to ensure minimal temperature and *p*H variation. Constant chemical conditions (implied by Ca^{2+} and alkalinity concentrations) were maintained by stoichiometric titration of reagent species (Romanek et al., 1992). Additionally, a constant pCO_2 ([gas phase] percent CO_2) was maintained during chemo-stat carbonate precipitation, which minimizes the potential for kinetically controlled fractionation due to CO_2 degassing or (de)hydration (Affek et al., 2008; Affek & Zaarur, 2014; Daëron et al., 2011; Guo, 2008). Carbonate precipitation was initiated by the introduction of pure calcite seed crystals to a slightly supersaturated solution (Figure 1), which induced heterogeneous growth and avoided the complications that arise from nucleation and growth under high supersaturation and mixed reaction mechanism kinetics. The mass of newly formed carbonate overgrowth was determined in two ways. The first was by mass difference between added seed crystals and final total calcite mass, although this method has the disadvantage of potential mass loss during sample handling. The second, and more precise approach, for determining the mass of carbonate overgrowth used an isotope dilution method (Faure & Mensing, 2009; Gagnon et al., 2012) by incorporating a ^{43}Ca-enriched tracer in the seed crystals (supporting information Table S1). This method allowed subtraction of seed crystal mass through measurement of Ca isotope compositions. Supporting information Table S3 provides a comparison of overgrowth

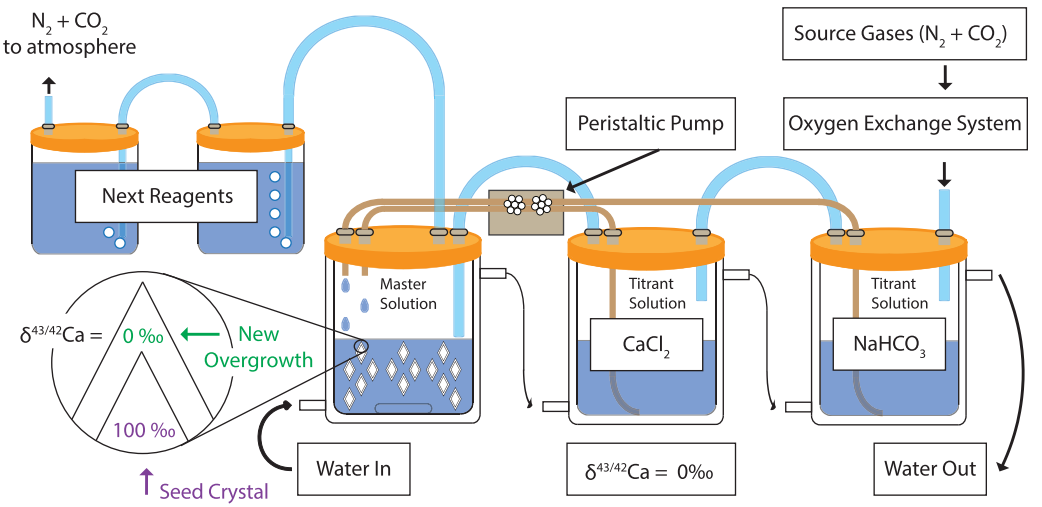

Figure 1. Schematic of chemo-stat experimental setup illustrating seed crystal and overgrowth details. The source of alkalinity used for these experiments was $NaHCO_3$. The C and O isotopes of the alkalinity produced by this reagent were defined by dissolving $NaHCO_3$ in stock DI water and bubbling with a CO_2/N_2 mixture several (4–10) days before being used to precipitate calcite. Before entering the fresh (sodium) bicarbonate solution, the CO_2/N_2 mixture was used to moderate the *p*H of a different actively precipitating master solution. In this way, a fresh solution was thoroughly flushed with "reagent" CO_2 (i.e., CO_2 that had been treated in the CO_2-H_2O exchange system) prior to use.

correction by mass balance and isotope dilution, and supporting information Table S2 provides analytical details of standards and equilibrated gases analyzed for Δ_{47}, as well as the calcite seed crystals. Corrections or conversions made based on these materials are described in supporting information text. Once the mass of overgrowth was determined, mixing calculations (Affek & Eiler, 2006) were used to calculate the Δ_{47} values of overgrowth carbonate. We note that because the seed crystals were synthesized at 20°C, and therefore had essentially the same Δ_{47} values as the overgrowth, the correction is very small for 20°C experiments. The corrections are larger for the 10°C and 30°C experiments. In all cases, uncertainties in the calculated Δ_{47} of newly grown carbonate include propagated errors in both measured Δ_{47} of seeds and overgrowths, and in the mixing ratio of seeds to overgrowths.

2.1. Inorganic Calcite Precipitation

Experiments were conducted at 10°C, 20°C, and 30°C for approximately 70 to 240 h. Calcite was formed from approximately 10 mM solutions of Ca^{2+} and HCO_3^- at *p*H values between 6.3 and 7.0. Chemo-stat conditions during calcite precipitation were maintained by titrating a master reaction vessel with separate solutions of $NaHCO_3$ and $CaCl_2$ that were independently added. The master solution was prepared by mixing 250 mL of individual $CaCl_2$ and $NaHCO_3$ titrant solutions which had been bubbled with pure CO_2 for approximately 1 h at room temperature to decrease the *p*H prior to master solution formation so that the mixture would be undersaturated with respect to $CaCO_3$. Soon after mixing, the master solution and new titrant solutions were incorporated into the experimental setup as shown in Figure 1 and introduced to a CO_2/N_2 gas mixture atmosphere as described to allow DIC and pCO_2 to reach a steady state at the desired supersaturation. Master solution *p*H and temperature were monitored during this equilibration period (normally several hours) and after approximately 1 h of stable *p*H, the experiment was initiated by introduction of seed crystals and commencement of titration. During experimentation, the solution chemistry was further stabilized by maintaining a constant *p*H via CO_2/N_2 flowing through the master solution reaction vessel. The partial pressure of CO_2 was established by mixing pure CO_2 and N_2 to total mixing ratios as indicated in Table 1. As an example, a pCO_2 of 15% was achieved by combining flow of 15 mL/min of CO_2 and 85 mL/min of N_2. Most calculated CO_2 partial pressures were within 1% of values set by mass-flow controllers and all values average an offset of -0.1%. The O isotope composition of reagent DIC ($NaHCO_3$) was allowed to exchange with the starting master or titration solution H_2O (see Figure 1) at low *p*H for 4–10 days depending on the length of the previous experiment at room temperature and then an additional several hours at the temperature of experimentation (see supporting information text for further details). This precaution circumvented the need (if any; Kelson et al., 2017) to use carbonic anhydrase for O isotope equilibration (Uchikawa & Zeebe, 2012; Watkins et al., 2013).

Calcite was precipitated in 1 L Pyrex containers that had been custom fitted with glass flow-through style jackets for temperature control (Figure 1). Titrant solutions were likewise jacketed and temperature controlled. Water was circulated by a heating/refrigerating water bath. The reaction vessel was mixed using a magnetic stir bar during carbonate formation. Experiments were designed to produce up to 160 mg of overgrowth carbonate on 80 mg of seed crystals. Master solution titration began immediately upon addition of seed crystals and ended shortly before product collection. Carbonate from the master solution was collected by decanting the reaction fluid into a 0.4 μm filtered vacuum system. The reaction vessel and calcite seeds were rinsed with DI water during filtration to prevent the formation of chloride salts. A small amount of methanol was used to help remove adsorbed water during filtration prior to further drying in an oven at 40°C for approximately 24 h. Following oven drying, the experimental product was checked for mineralogy by XRD and then stored in a Dri-Rite filled desiccator until analysis.

2.2. Experimental Conditions

Temperature and precipitation rate were the primary variables explored. Three temperatures were investigated: 10°C, 20°C, and 30°C, and these temperatures were controlled to within $\pm$1°C during carbonate formation using a water-jacketed vessel. Temperature was measured with a thermocouple integrated with the Cole-Parmer electrode and the time-weighted standard deviation during mineral growth was $\sim$0.1°C. The CO_2-H_2O exchange system (Levitt & Romanek, 2016) was also maintained at the experimental reaction temperature during CO_2 conditioning. Most reagent solutions were flushed with effluent CO_2/N_2 prior to use to replace the C isotope composition of $NaHCO_3$ reagent (see supporting information text for details). Carbonate precipitation rates (moles m^{-2} s^{-1}) were varied by changing the rate of titrant solutions to the master

Table 1
Experimental Conditions and Supporting Isotope Compositions

Experiment identification	Experiment length (h)	Temperature (°C)[a]	pCO_2 (%)	pH	Ca^{2+} (mmol)	Alkalinity (meq)	Saturation Ω	log rate (mol m^{-2} s^{-1})	Water $\delta^{18}O$ (‰, VSMOW)	DIC $\delta^{13}C$ (‰, VPDB)	HCO_3^- $\delta^{13}C$ (‰, VPDB)
UWAI-016	94	9.9	10	6.5	9.7	8.9	1.1	−7.54	−8.9	−2.0	2.0
UWAI-017	93	9.9	10	6.6	9.7	8.8	1.1	−7.53	−8.8	−1.9	1.5
UWAI-018	138	10.0	10	6.5	9.8	8.7	1.1	−7.63	−9.0	−2.0	1.9
UWAI-019	136	9.9	10	6.7	10.1	8.7	1.5	−7.60	−8.9	−1.9	1.0
UWAI-025	206	9.5	6	6.7	10.3	7.8	1.3	−8.10	−8.8	−3.4	−0.5
UWAI-026	204	10.4	6	6.8	10.4	7.9	1.7	−8.10	−8.9	−3.2	−0.7
UWAI-027	180	10.0	6	6.8	10.3	8.0	1.7	−8.19	−8.9	−3.5	−0.9
UWAI-028	178	10.0	6	6.8	10.4	8.1	1.8	−8.20	−9.0	−3.4	−0.8
UWAI-029	69	10.0	6	6.8	10.1	8.3	1.8	−7.63	−9.1	−2.7	−0.1
UWAI-030	68	10.9	6	6.8	10.0	8.5	1.8	−7.70	−9.1	−2.9	−0.6
UWAI-031	232	9.8	6	6.7	10.3	9.1	1.5	−8.04	−9.1	−4.2	−1.1
UWAI-032	227	9.9	6	6.7	10.5	9.4	1.6	−8.11	−8.9	−4.0	−1.0
UWAI-033	117	9.9	6	6.8	10.4	8.5	1.8	−7.47	−8.8	−2.5	0.0
UWAI-034	115	10.5	6	6.8	10.4	8.6	1.9	−7.48	−8.7	−2.4	0.0
UWAI-002	151	20.0	5	6.8	10.1	7.9	2.3	−7.45	−8.9	−2.8	−0.9
UWAI-003	143	20.0	5	6.9	10.4	8.1	3.1	−7.55	−9.1	−2.9	−1.3
UWAI-004	144	20.0	5	6.9	10.0	8.1	3.0	−7.51	−8.9	−2.8	−1.2
UWAI-005	191	20.0	5	6.9	10.6	7.9	3.0	−7.65	−8.9	−3.3	−1.7
UWAI-006	93	20.0	5	6.9	10.0	8.1	3.0	−7.24	−8.7	−2.8	−1.2
UWAI-007	91	19.9	5	6.8	10.6	6.7	2.1	−7.25	−8.7	−2.6	−0.8
UWAI-008	95	20.0	5	6.9	9.7	8.1	2.9	−7.23	−8.6	−3.0	−3.1
UWAI-009	94	19.9	5	6.9	10.0	8.0	2.9	−7.27	−8.8	−2.8	−1.2
UWAI-010	193	20.0	5	6.9	9.8	7.8	2.8	−7.64	−8.8	−3.0	−1.3
UWAI-011	191	19.9	5	7.0	9.8	7.8	3.5	−7.59	−8.9	−2.9	−1.5
UWAI-012	109	20.0	5	7.0	9.9	8.2	3.7	−7.38	−8.8	−2.5	−1.1
UWAI-013	101	19.9	5	7.0	10.1	8.3	3.8	−7.44	−8.9	−2.5	−1.1
UWAI-014	91	20.0	10	6.6	10.1	9.1	1.7	−7.50	−8.7	−3.4	−1.7
UWAI-015	89	19.9	10	6.6	10.5	9.2	1.7	−7.59	−8.8	−3.0	−0.5
UWAI-023	137	20.0	6	6.8	8.1	8.8	2.2	−7.00	−8.2	−3.2	−1.3
UWAI-024	138	19.9	6	6.9	8.6	9.0	2.9	−6.88	−8.3	−3.4	−1.7
UWAI-045	200	19.6	13	6.5	11.0	9.2	1.4	−7.92	−8.7	−4.7	−1.7
UWAI-046	198	19.8	13	6.5	11.2	9.2	1.4	−7.82	−9.0	−5.0	−1.9
UWAI-020	119	30.0	16	6.3	9.9	8.0	1.3	−7.40	−8.9	−5.5	−2.0
UWAI-021	121	30.1	16	6.5	9.8	8.6	1.7	−7.47	−8.6	−6.0	−3.5
UWAI-035	149	30.0	13	6.6	10.3	8.0	2.0	Unknown[a]	−8.9	−5.1	−2.7
UWAI-036	143	30.2	13	6.6	10.6	8.5	2.2	−7.51	−8.9	−4.6	−2.5
UWAI-037	235	29.9	13	6.5	10.2	7.9	1.6	−7.65	−8.5	−4.9	−2.4
UWAI-038	233	29.9	13	6.5	10.3	7.9	1.6	−7.66	−8.6	−5.0	−2.6
UWAI-039	89	30.0	13	6.5	10.5	8.0	1.6	−7.25	−8.6	−5.0	−2.5
UWAI-040	87	30.1	13	6.6	10.9	8.7	2.3	−7.37	−8.7	−4.5	−2.5
UWAI-041	144	30.0	13	6.5	10.6	8.3	1.7	−7.42	−9.0	−4.9	−2.3
UWAI-042	142	30.0	13	6.5	10.6	8.3	1.7	−7.47	−9.2	−4.5	−2.0
UWAI-043	240	30.0	13	6.5	10.6	8.4	1.7	−7.72	−8.7	−5.3	−2.6
UWAI-044	238	30.2	13	6.6	11.0	9.1	2.4	−7.88	−8.8	−4.4	−2.2
UWAI-047	214	29.5	13	6.5	11.2	8.3	1.7	−7.92	−9.1	−6.6	−4.1
UWAI-048	211	30.2	13	6.5	11.2	8.6	2.3	−7.82	−9.5	−6.5	−4.2

[a]Experiment UWAI-035 homogeneously nucleated, UWAI-036 rate used in figures.

solution (Figure 1) for various experimental times. The desired length of a given experiment determined the titration rate needed to add ~250 mL of each titrant solution. In all cases, low supersaturation states (2–4 times saturation) were used to remain as close to equilibrium conditions as possible (Watkins & Hunt, 2015; Wolthers, et al., 2012). Actual values in this range were dictated by the accuracy to which pCO_2 could be set by mass-flow controllers (0.2 to 10 ± 0.5% mL min^{-1} for CO_2 and 20 to 1,000 ± 0.5% mL min^{-1} for N_2). Master and titrant solutions were prepared such that concentrations of Ca^{2+} and alkalinity would be 10 mM and 10 milliequivalents (meq) in the master solution during carbonate precipitation. Actual solution concentrations were measured before and after each experiment (see supporting information Table S1 and

supporting information text for full details). Saturation states were modeled with PHREEQC software (Parkhurst & Appelo, 2013) and phreeqc.dat database before and after an experiment.

2.3. Geochemical Analyses and Notation

Stable Ca isotope analysis, XRD, surface area measurements, and determination of solution chemistries were performed at the University of Wisconsin—Madison. Bulk C, bulk O, and clumped isotope compositions for calcite were determined at the California Institute of Technology by isotope ratio mass spectrometry on both of two nearly identical Thermo-Finnigan MAT 253 instruments. Oxygen isotope compositions of solution H_2O, as well as C isotope compositions of DIC, were analyzed at the University of California—Davis. Values of $\delta^{13}C$ reported in this investigation are with respect to international standard Vienna Peedee Belemnite (VPDB), and $\delta^{18}O$ values are with respect to Vienna Standard Mean Ocean Water (VSMOW). Clumped isotope compositions are described in terms of the Absolute Reference Frame (ARF) as described by Dennis et al. (2011). See supporting information text for full details, including methodologies (Brand et al., 2010; Daeron et al., 2016; Olack & Coleman (2016), Santrock et al., 1985; and Schauer et al., 2016) as well as precision and accuracy considerations.

Calcium was prepared prior to isotope analysis by ion-exchange chromatography similar to that reported by Li et al. (2012). Approximately 0.25 mg of calcite or 2.5 mL of reaction solution was processed for Ca isolation. Calcite was dissolved in dilute ultrapure nitric acid and converted to pure $Ca(NO_3)_2$ before purification. Likewise, nitric acid was added to experimental solutions and dried until only solids remained. These solids were repeatedly dissolved with nitric acid and redried three times to ensure all cations were transformed into nitrate salts. Calcium was isolated and purified from other cations by ion-exchange chromatography before isotope analysis. Calcium isotope analyses were performed using a Micromass IsoProbe MC-ICP-MS at the University of Wisconsin-Madison. Helium was used as the collision gas for thermalization and H_2 was used to suppress argide isobars by charge-transfer reactions. Calcium solution concentrations of 10 ppm were introduced to the Ar plasma using a self-aspirating 50–100 μL min^{-1} nebulizer coupled to a Cetac Aridus II membrane desolvating system. The cone voltage was set to 200–500 V. These settings allowed Ca ion intensities of 44.5, 0.34, 0.07, and 1.22 V at mass numbers 40, 42, 43, and 44, respectively. A 2% HNO_3 solution was used as a rinse solution between individual sample measurements. The sample solutions were also measured using a standard-sample-standard bracketing protocol. Concentration-related matrix effects were corrected according to standard solutions ranging from 5 to 15 ppm Ca, as outlined by Albarède and Beard (2004).

Carbonate C and O isotope analyses as well as clumped isotope analyses were performed on two Thermo-Finnigan MAT 253 (Thermo Scientific, Bremen, Germany) isotope ratio mass spectrometers according to the procedures outlined by Passey et al. (2010). A single analysis consisted of digestion of 8–10 mg calcite in a common phosphoric acid bath at 90°C followed by an automated CO_2 cleaning and purification process. See Passey et al. (2010) for automation and sample preparation details. Carbon and O isotope ratios for sample and standard material were determined by Isodat software with comparison to an Oztech reference gas of known isotope composition. An O isotope acid fractionation factor of 1.00821 (Swart et al., 1991) was used to correct gas phase CO_2 back to calcite $\delta^{18}O$ values. A clumped isotope value of 0.082‰ was used to correct for acid digestion (Deflies et al., 2015). In addition to unknown samples, standard reference material was also analyzed in tandem during each analytical session.

Oxygen isotope ratios for water were determined using a Laser Water Isotope Analyzer V2 (Los Gatos Research, Inc., Mountain View, CA, USA) and standardized using working materials that were calibrated to International Atomic Energy Agency standard reference materials VSMOW, Greenland Ice Sheet Precipitation (GISP), and Standard Light Antarctic Precipitation (SLAP). DIC C isotope analyses utilized a Delta V Plus (Thermo Scientific, Bremen, Germany) isotope ratio mass spectrometer to determine ratios of evolved trace gas phase CO_2. The IRMS system was interfaced with a Finnigan Gasbench II device for sample preparation and transfer. DIC analysis was similarly standardized according to materials traceable to National Institute of Standards and Technology reference material 8545.

Errors given in Table 2 and throughout the paper represent two standard deviations about the mean for measured values. Propagated errors for derivative values such as precipitation rates and fractionation factors are determined as the square root of the sum of the squares. Isotopic compositions in supporting information Table S3 that consider overgrowth mass uncertainty are presented as the difference between the

Table 2
Isotope Compositions of Carbonate Overgrowth and Phase Fractionations

	Experiment identification	System T (°C)	Calcite $\delta^{13}C$ (‰, VPDB)	Calcite $\delta^{18}O$ (‰, VSMOW)	Δ_{47} (‰, ARF)	$\Delta^{13}C_{calcite\text{-}HCO_3O^-}$ (‰)[b]	$\Delta^{18}O_{calcite\text{-}H_2O}$ (‰)
Experiments performed at 10°C	UWAI-016	9.9	1.2 ± 0.1	23.7 ± 0.5	0.797 ± 0.017	−0.7 ± 0.1	32.3 ± 0.6
	UWAI-017	9.9	1.4 ± 0.3	23.5 ± 0.4	0.773 ± 0.035	−0.2 ± 0.3	32.2 ± 0.5
	UWAI-018	10.0	1.4 ± 0.2	23.8 ± 0.4	0.777 ± 0.046	0.2 ± 0.2	32.5 ± 0.5
	UWAI-019	9.9	1.3 ± 0.1	23.8 ± 0.3	0.768 ± 0.052	0.6 ± 0.1	32.5 ± 0.5
	UWAI-025	9.5	1.5 ± 0.4	24.0 ± 0.4	0.741 ± 0.021	**1.6 ± 0.4**	32.6 ± 0.7
	UWAI-026	10.4	1.4 ± 0.6	24.0 ± 0.4	0.760 ± 0.035	**1.6 ± 0.6**	32.6 ± 0.8
	UWAI-027	10.0	1.2 ± 0.6	24.1 ± 0.4	0.779 ± 0.040	**1.7 ± 0.6**	32.7 ± 0.4
	UWAI-028	10.0	1.3 ± 1.2	23.8 ± 0.6	0.796 ± 0.070	**1.8 ± 1.2**	32.6 ± 0.6
	UWAI-029	10.0	1.5 ± 0.3	23.9 ± 0.5	0.748 ± 0.066	**1.4 ± 0.3**	32.8 ± 0.5
	UWAI-030	10.9	1.5 ± 0.4	23.9 ± 0.6	0.750 ± 0.080	**1.7 ± 0.4**	32.8 ± 0.6
	UWAI-031	9.8	0.3 ± 0.4	23.8 ± 0.4	0.742 ± 0.039	**1.6 ± 0.4**	32.7 ± 0.4
	UWAI-032	9.9	0.9 ± 0.6	23.9 ± 0.4	0.766 ± 0.060	**1.4 ± 0.6**	32.6 ± 0.4
	UWAI-033	9.9	1.6 ± 0.2	23.7 ± 0.4	0.754 ± 0.082	**1.5 ± 0.2**	32.3 ± 0.5
	UWAI-034	10.5	1.7 ± 0.3	23.7 ± 0.2	0.756 ± 0.051	**1.5 ± 0.3**	32.2 ± 0.3
	Average	**10.1**			**0.765 ± 0.036**	**1.6 ± 0.2**	**32.5 ± 0.4**
Experiments performed at 20°C	UWAI-002	20.0	−0.5 ± 0.5	21.2 ± 0.4	0.732 ± 0.080	0.0 ± 0.5	30.0 ± 0.5
	UWAI-003	20.0	−0.4 ± 0.3	21.2 ± 0.1	0.726 ± 0.083	−0.1 ± 0.3	30.1 ± 0.4
	UWAI-004	20.0	0.1 ± 0.1	21.6 ± 0.05	0.719 ± 0.010	0.4 ± 0.1	30.3 ± 0.3
	UWAI-005	20.0	0.0 ± 0.1	21.5 ± 0.2	0.726 ± 0.049	**1.7 ± 0.1**	30.2 ± 0.4
	UWAI-006	20.0	0.7 ± 0.1	21.5 ± 0.1	0.729 ± 0.077	**1.9 ± 0.2**	30.0 ± 0.4
	UWAI-007	19.9	0.5 ± 0.5	21.6 ± 0.5	0.726 ± 0.065	**1.2 ± 0.6**	30.1 ± 0.6
	UWAI-008	20.0	0.4 ± 0.03	21.4 ± 0.6	0.721 ± 0.055	0.4 ± 0.1	29.8 ± 0.7
	UWAI-009	19.9	0.4 ± 0.2	21.3 ± 0.4	0.726 ± 0.055	−0.6 ± 0.2	29.9 ± 0.6
	UWAI-010	20.0	0.8 ± 0.5	21.6 ± 0.4	0.749 ± 0.028	**1.9 ± 0.5**	30.1 ± 0.5
	UWAI-011	19.9	−0.1 ± 1.4	21.5 ± 0.2	0.748 ± 0.054	**1.1 ± 1.4**	30.2 ± 0.4
	UWAI-012	20.0	0.4 ± 0.1	21.5 ± 0.4	0.744 ± 0.060	**1.4 ± 0.1**	30.1 ± 0.5
	UWAI-013	19.9	0.6 ± 0.1	21.6 ± 0.5	0.735 ± 0.044	**1.6 ± 0.1**	30.3 ± 0.6
	UWAI-014	20.0	1.1 ± 0.3	21.7 ± 0.3	0.729 ± 0.057	**1.7 ± 0.3**	30.2 ± 0.5
	UWAI-015	19.9	0.5 ± 0.2	21.6 ± 0.5	0.717 ± 0.046	**1.3 ± 0.2**	30.2 ± 0.6
	UWAI-023	20.0	0.2 ± 0.3	21.3 ± 0.1	0.707 ± 0.085	**1.3 ± 0.3**	29.4 ± 0.2
	UWAI-024	19.9	0.3 ± 0.3	21.3 ± 0.04	0.735 ± 0.056	**1.7 ± 0.3**	29.4 ± 0.1
	UWAI-045	19.6	0.5 ± 0.2	21.6 ± 0.3	0.733 ± 0.054	**1.8 ± 0.5**	30.4 ± 1.0
	UWAI-046	19.8	0.5 ± 0.3	21.6 ± 0.4	0.731 ± 0.115	**1.8 ± 0.3**	30.4 ± 0.4
	Average	**19.9**			**0.729 ± 0.021**	**1.6 ± 0.5**	**30.1 ± 0.7**
Experiments performed at 30°C	UWAI-020	30.0	−1.1 ± 0.3	19.2 ± 0.6	0.703 ± 0.014	0.4 ± 0.3	27.9 ± 0.7
	UWAI-021	30.1	−0.5 ± 0.4	19.5 ± 1.1	0.721 ± 0.067	1.5 ± 0.4	28.0 ± 1.1
	UWAI-035[a]	30.0	−1.0 ± 0.1	19.2 ± 0.1	0.674 ± 0.077	**2.0 ± 0.2**	28.0 ± 0.1
	UWAI-036	30.2	−0.5 ± 0.3	19.5 ± 0.4	0.672 ± 0.053	**1.6 ± 0.3**	28.2 ± 0.4
	UWAI-037	29.9	−0.9 ± 0.3	19.4 ± 0.5	0.672 ± 0.127	**1.4 ± 0.3**	27.8 ± 0.6
	UWAI-038	29.9	−0.9 ± 0.2	19.3 ± 0.4	0.688 ± 0.077	**1.5 ± 0.2**	27.8 ± 0.4
	UWAI-039	30.0	−0.8 ± 0.4	19.5 ± 0.6	0.679 ± 0.129	**1.5 ± 0.4**	27.9 ± 0.6
	UWAI-040	30.1	−0.1 ± 0.3	19.6 ± 0.4	0.696 ± 0.080	**1.8 ± 0.3**	28.1 ± 0.5
	UWAI-041	30.0	−0.8 ± 0.2	19.4 ± 0.3	0.690 ± 0.108	**1.5 ± 0.2**	28.3 ± 0.3
	UWAI-042	30.0	−0.9 ± 0.1	19.3 ± 0.4	0.688 ± 0.096	**1.3 ± 0.1**	28.4 ± 0.4
	UWAI-043	30.0	−0.7 ± 0.2	19.4 ± 0.4	0.712 ± 0.066	**1.5 ± 0.2**	28.0 ± 0.4
	UWAI-044	30.2	−0.3 ± 0.2	19.5 ± 0.6	0.717 ± 0.129	**1.5 ± 0.2**	28.2 ± 0.6
	UWAI-047	29.5	−0.6 ± 0.4	19.6 ± 0.3	0.687 ± 0.105	2.8 ± 0.5	28.5 ± 0.3
	UWAI-048	30.2	−1.3 ± 0.3	19.0 ± 0.5	0.650 ± 0.115	2.9 ± 0.3	28.3 ± 0.5
	Average	**30.0**			**0.689 ± 0.039**	**1.6 ± 0.4**	**28.1 ± 0.5**

[a]Experiment UWAI-035 homogeneously nucleated. [b]$\Delta^{13}C_{calcite\text{-}HCO_3^-}$ values in bold are representative of experimental conditions, see text for details. Error values represent 2 standard deviations about the mean of multiple (≥3) analyses.

determined overgrowth mass and the 2σ maximum and minimum overgrowth. The expression used to calculate C and O isotope composition of overgrowth carbonate is

$$\delta_o = \frac{(\delta_{tot} - \delta_s(1-\chi))}{\chi} \quad (1)$$

where δ_o is the isotope composition of the overgrowth, δ_{tot} is the measured isotope composition of the overgrowth plus seed crystals, δ_s is the isotope composition of the seed crystals, and χ is the mass fraction of overgrowth to final total carbonate. While this equation is not exact because it assumes linearity in terms of δ notation, tabulated values are accurate to 0.03‰ for the range of $\delta^{13}C$ and $\delta^{18}O$ values reported here, and hence do not significantly affect corrected δ values.

Bulk stable isotope compositions (C, O, and Ca) are reported in units of per mil (‰) in standard form:

$$\delta^n X = \left(\frac{R_{sa} - R_{std}}{R_{std}}\right) \times 10^3 \quad (2)$$

where n is 13 (C), 18 (O), or 43 (Ca), X is the element of interest, R_{sa} is the isotope ratio of the sample, and R_{std} is the isotope ratio of a reference standard. Similarly, the convention for describing the magnitude of clumping in a sample is given by the Δ_i value (also in units of per mil) where i is the atomic mass of the isotopologue of interest. Examples include Δ_{47} for $^{13}C^{18}O^{16}O$ and Δ_{63} for $^{13}C^{18}O^{16}O_2^{2-}$. Measured Δ_{47} values do not, however, exactly equal the deviation in $^{13}C^{18}O^{16}O$ species relative to random distribution, as a small fraction of very rare isotopologues also have a mass of 47, although these are unimportant at the current level of precision. Δ_i is defined as

$$\Delta_i = \left(\frac{R_i - R_{i^*}}{R_{i^*}}\right) \times 10^3 \quad (3)$$

where R_i is the abundance ratio of the isotopologue of interest and R_i^* is an analogous ratio for a population of isotopologues that has the same bulk isotopic composition but a stochastic distribution (Huntington et al., 2009). Both ratios are relative to the most abundant isotopologue ($^{12}C^{16}O_2$ and $^{12}C^{16}O_3^{2-}$). Clumped isotope values (Δ_{47}) have been corrected for the seed crystal isotope compositions (bulk and clumped as presented in supporting information Table S3) according to the nonlinear mixing equations of Affek and Eiler (2006) and reported values only represent overgrowth.

The partitioning of isotopes between two phases is described here as

$$10^3 \ln(\alpha_{a-b}) = 10^3 \ln\left(\frac{1,000 + \delta_a}{1,000 + \delta_b}\right) \approx \delta_a - \delta_b \quad (4)$$

where α_{a-b} is defined as the fractionation factor between the two phases (a and b) and δ_a and δ_b are the isotope compositions of the two phases ($\delta^{13}C$ and $\delta^{18}O$).

The saturation state convention of Morse and Mackenzie (1990) is used throughout the paper and defined as

$$\Omega_{calcite} = \frac{a_{Ca^{2+}} * a_{CO3^{2-}}}{K_{calcite}} \quad (5)$$

where a denotes the activity of an ionic species and K is the solubility product. Activities and saturation were determined by PHREEQC (Parkhurst & Appelo, 2013) software. The reference state solubility product for calcite in the phreeqc.dat database is $K = 10^{-8.48}$.

3. Results

3.1. Solution Chemistry and Product Carbonate Characterization

Table 1 lists the measured average Ca, alkalinity, pCO_2, and pH values, as well as calculated saturation states for all experiments performed during this study. Starting and ending master solutions were analyzed to verify minimal solution chemistry variation during the experiments. The average of starting and ending aqueous Ca concentrations ranged from 8.1 to 11.2 ± 1.1 mmol L^{-1}. Similarly, alkalinity concentrations were 6.7 to 9.4 ± 0.07 meq. Time-weighted pH average values were between 6.3 and 7.0 ± 0.07 pH units. These pH values were established in part by pCO_2 concentrations in the 5–16% range during the experiments. Additionally, a constant partial pressure of CO_2 (pCO_2, reported in terms of volume percent carbon dioxide) helped to minimized drift or fluctuation in solution conditions. These parameters produced saturation states with respect to calcite of 1.1 to 3.8 ± 0.01.

The average mass of overgrowth calcite per experiment was approximately 141 mg (supporting information Table S1), which compares to the average mass of seed crystal used of 80.4 mg per experiment. Variation in overgrowth mass between experiments is believed to be due to the small amount of saturation state variability and/or small differences (~50 mL) in the actual amount of titrant solution added to the master solution at the end of each experiment. Isotope dilution calculations for the mass of overgrowth have an average uncertainty of ±2.9% (~4 mg), as determined by the 2-standard deviation value (±1.07‰) about the mean of in-house Ca standard solutions analyzed during ending master solution isotope composition characterization. For Δ_{47} values, this error translates to a propagated maximum average uncertainty due to overgrowth of ±0.017‰, which is less than the 2-SD external precision (standard deviation about the mean) determined for Δ_{47} analyses of carbonate standards (±0.034‰). The uncertainty in Δ_{47} values reported in Table 2 accounts for overgrowth as well as measurement replication. Errors for each analysis associated with isotopic composition measurement and overgrowth correction are given in supporting information Table S3.

The Ca isotope composition was also measured for each master solution after calcite filtration was performed. This analysis was intended to identify any dissolution of seed crystals during the experiments, which was a possibility given the low saturation state of the experiments. Measured Ca isotope compositions of final solutions were within error of starting master solutions for all but five experiments, where the calculated mass of dissolved seed crystals ranged from 7.0 to 15.8 mg, which is equivalent to dissolution of ~3.8–10.7% of the seed crystals, indicating that these experiments involved some dissolution (possibly due to stir bar grinding and/or Ostwald ripening) despite net growth of new calcite. Although such results provide insights into the dynamic nature of the calcite interface during precipitation, they do not affect the calculated Δ_{47} values for the overgrowths because all five of the experiments that showed minor seed crystal dissolution were performed at 20°C, and hence the Δ_{47} values for the seed crystals were essentially identical to the overgrowths. Therefore, these five experiments remain included in the data set.

Overgrowth carbonate mineralogy was verified by microscopic inspection as well as XRD. A representative SEM image and XRD patterns are provided in supporting information (Figures S1 and S2). In all cases, only calcite was identified in reaction products. Seed calcite was further characterized by BET surface area analysis (Brunauer et al., 1938) to be 1.2 ± 0.2 $m^2\ g^{-1}$. This value was used to determine precipitation rates, in conjunction with calcite masses (seed and overgrowth), and experiment length. Precipitation rates used during these experiments ranged from 0.006 to 0.034 μmol $m^{-2}\ s^{-1}$ for 10°C experiments, from 0.012 to 0.132 μmol $m^{-2}\ s^{-1}$ for 20°C experiments, and from 0.012 to 0.056 μmol $m^{-2}\ s^{-1}$ for 30°C experiments. Error-propagated uncertainties for precipitation rates ranged between 2% and 19%.

3.2. Isotopic Analyses

$\delta^{13}C$ values for overgrowth carbonate ranged from −1.3‰ to 1.7‰, and $\delta^{18}O$ values for overgrowth carbonate ranged from 19.0‰ to 24.1‰ (Table 2). The C isotope composition of starting and ending master solution DIC is reported in supporting information Table S1, and $\delta^{13}C$ values for DIC ranged from −6.6‰ to −1.5‰. Likewise, the O isotope composition of master solution water is given in Table 1 and ranged from $\delta^{18}O$= −9.5‰ to −8.2‰. Most ending solutions were within 0.3‰ of starting master solution values, confirming maintenance of chemo-stat conditions in terms of isotopic composition. Individual starting and ending master solution values are presented in supporting information Table S1.

Measured O and C isotope compositions allowed for determination of fractionation factors between calcite and water as well as between calcite and calculated values of individual DIC species. Average $^{18}O/^{16}O$ fractionations between calcite and water ($10^3 ln\alpha_{CC\text{-}H_2O}$) at 10°C, 20°C, and 30°C were found to be 32.5 ± 0.4‰, 30.0 ± 0.7‰, and 28.1 ± 0.5‰, respectively. Bicarbonate (HCO_3^-) isotope compositions were calculated from measured DIC $\delta^{13}C$ values and used to determine the $^{13}C/^{12}C$ fractionation factors between calcite and bicarbonate($10^3 ln\alpha_{CC\text{-}HCO_3}$), which, at 10°C, 20°C, and 30°C, were 1.6 ± 0.2‰, 1.6 ± 0.5‰, and 1.6 ± 0.4‰, respectively. Uncertainty in $10^3 ln\alpha$ values represents 2SD external error and seed crystal subtraction. Average fractionation factors only consider experiments that used titrant solutions that had been appropriately preflushed with a N_2/CO_2 gas mixture (see "Next Reagents" section of Figure 1 and the supporting information text). Specifically, the titrants for experiments UWAI-002, UWAI-003, UWAI-004, UWAI-008, and UWAI-009 were not treated with a N_2/CO_2 gas mixture before use. Additionally, UWAI-016 through UWAI-021, as well as UWAI-047 and UWAI-048, were treated at a different temperature than the temperature at which

they were used during experimentation. For example, if reagents were flushed with CO_2 exiting a 20°C experiment and then those reagents were used for 10°C experiments, their $\alpha_{CaCO_3-HCO_3}$ values were found to be systematically different from values obtained where temperature of flushing and experimental temperature was the same. This observation is believed to reflect a fractionation in C isotopes between gas phase and DIC that was subsequently transferred to the reagent alkalinity used for experiments. These relations are observable in Table 2. Values in bold font average to 1.6‰.

Clumped isotope compositions for overgrowth calcite are presented in Table 2. Additional details regarding standards, heated gasses, and equilibrated gasses analyzed during the same sessions as experimental samples (given in supporting information Table S2), whereas information related to raw uncorrected values for C, O, and clumped isotope analyses, which are with respect to an Oztech reference gas (the working gas used in the Caltech lab), are included in supporting information Table S3. The latter table also includes corrected clumped isotope values relative to the ARF, seed crystal contribution, and acid digestion fractionation. Clumped isotope compositions for overgrowth carbonate ranged from $\Delta_{47} = 0.742‰$ to 0.797‰ for 10°C experiments, from 0.707‰ to 0.749‰ for 20°C experiments, and from 0.650‰ to 0.721‰ for 30°C experiments. Average Δ_{47} values for 10°C, 20°C, and 30°C are $0.765 \pm 0.036‰$, $0.729 \pm 0.021‰$, and $0.689 \pm 0.039‰$, respectively. It is also worth noting that that the method used to form seed crystals has been reported to initially form amorphous calcium carbonate which transforms to vaterite and then calcite (Ogino et al., 1987; Rodriguez-Blanco et al., 2011; see supporting information text for details). However, despite this pathway, the Δ_{47} value of the seed calcite was found to be $0.735 \pm 0.024‰$ (n = 9) which is in good agreement with overgrowth values at this temperature. Uncertainty in Δ_{47} values represents 2SD external error (standard deviation about the mean) which also accounts for seed crystal subtraction.

4. Discussion

Our data set allows assessment of $^{13}C—^{18}O$ bonding with respect to equilibrium conditions from an O, C, and clumped isotope perspective as well as from a range of solution conditions. In addition to precipitation rate, *p*H and saturation effects have also been considered. We find no direct evidence relating *p*H variability to bulk isotope fractionation (or compositions), as well as no relation between $^{13}C—^{18}O$ bonding and *p*H. However, admittedly, our range of *p*H values is limited. $^{13}C—^{18}O$ bonding, conversely, is shown to increase with decreasing saturation state when multiple data sets are considered. Indirect factors (DIC speciation) related to *p*H are considered through the model of Watkins and Hunt (2015). This model was chosen for consideration due to its treatment of C, O, and clumping isotope partitioning in terms of precipitation rate, parallel to the focus of our study of precipitation rate effects. A detailed description of the Watkins and Hunt model can be found in supporting information text. As will be discussed below, we suggest that complete O isotope equilibrium between calcite and water has yet to be obtained for experimental synthesis of calcite, including the current study. Although the information presented here does not exclude the possibility of disequilibrium $^{13}C—^{18}O$ bonding under some precipitation rates as discussed below, we find no convincing evidence for this phenomenon in our data set. Our results do, however, add evidence to the argument that faster calcite precipitation and/or higher saturation states can allow kinetic isotope effects to influence the partitioning of C and O during carbonate mineral formation from solution, which is discussed below in more detail.

4.1. Carbon Isotopes

The rate dependence of C isotope fractionations among C species can provide insights into the potential kinetic effects in isotopic partitioning as related to DIC speciation based on equilibrium constants for the system CO_2-H_2O-DIC (Zeebe & Wolf-Gladrow, 2001). Watkins et al. (2014; see also Watkins & Hunt, 2015) explore kinetic isotope fractionation between ions in solution and solid phase carbonate during calcite precipitation, and conclude that deviations from equilibrium can be understood through differences in rates of solid formation versus isotope exchange between DIC species and water. More specifically, at very slow precipitation rates, isotope fractionation between DIC and calcite is a function of equilibrium partitioning between H_2O, HCO_3^-, CO_3^{2-}, and $CaCO_3$(s). At faster growth rates, however, as the kinetic limit is approached, the isotope composition of precipitating carbonate is determined by the ratio of HCO_3^- to CO_3^{2-} incorporation and kinetic fractionation factors between each species and the mineral phase. Such a model is based on assuming the equilibrium fractionation is recorded by the work of Coplen (2007) and

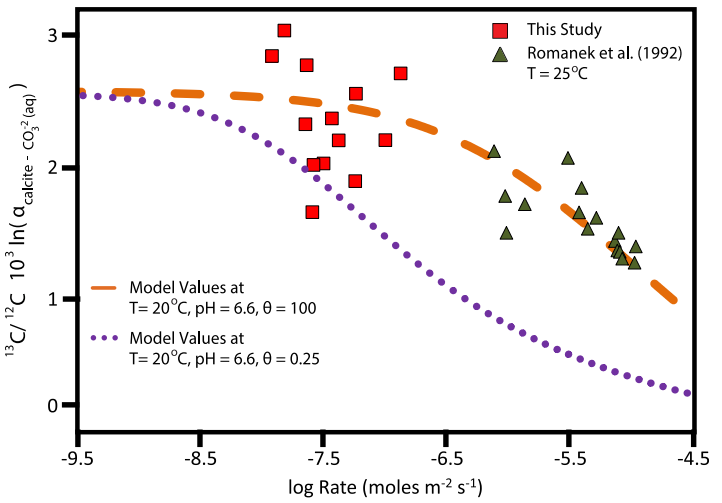

Figure 2. Reproduction of the semiempirical ion-by-ion growth model of Watkins and Hunt (2015) for C isotope fractionation during calcite growth under kinetic and (assumed) equilibrium conditions. The model is based on a "kinetic" regime from the experiments of Romanek et al. (1992, shown by green triangle symbols) and inferred equilibrium from Coplen (2007). The orange dashed line is the modeled fractionation for 20°C, *p*H = 6.6, and a surface HCO_3^-:CO_3^{2-} ratio (θ) of 100:1. The purple dotted line is modeled fractionation for 20°C, *p*H = 6.6, and a surface HCO_3^-:CO_3^{2-} ratio (θ) of 0.25:1. Also included are values found during this study at 20°C for partitioning between calcite and aqueous carbonate (red squares).

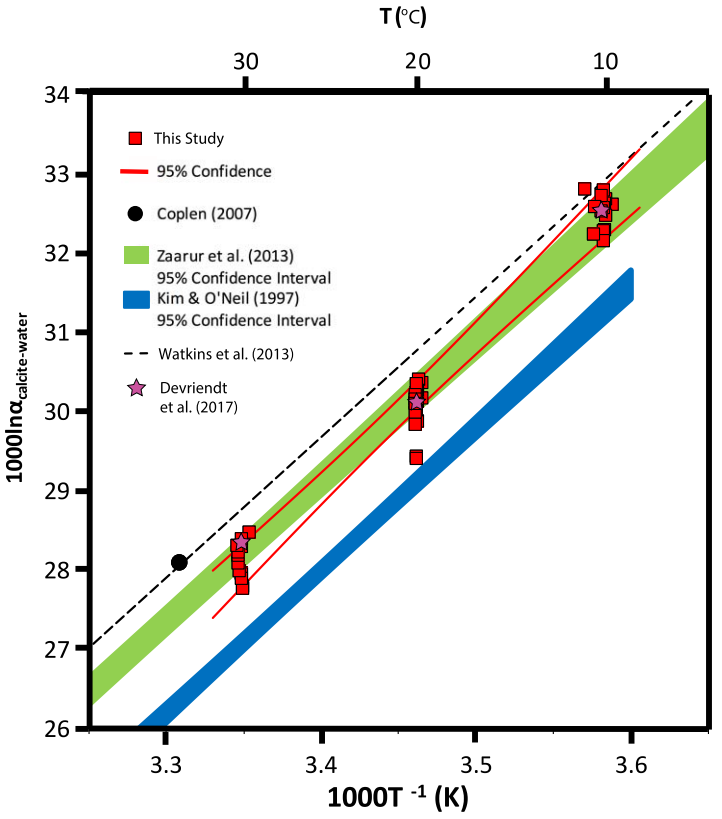

Figure 3. Observed temperature-dependent calcite-water O isotope fractionation found by this study as compared to other work. The black circle represents Devils Hole calcite (Coplen, 2007). The average propagated 2SD external uncertainty for experimental values is ±0.47‰. Individual values are given in Table 2.

Bottinga (1968) at a log value rate of $\sim\leq -9.5$ moles m^{-2} s^{-1}, as well as the kinetic fractionations inferred for C isotopes from Romanek et al. (1992).

In Figure 2, we model the kinetic effects on C isotope fractionation at 20°C, following the approach of Watkins and Hunt (2015), illustrating the isotope fractionation between calcite (cc) and aqueous CO_3^{2-}. Analogous figures for 10°C and 30°C are included in supporting information (Figures S3 and S4). When our results are compared with previous work of Romanek et al. (1992), reasonable agreement is observed over a range of precipitation rates in terms of the model of Watkins and Hunt (2015) using a surface speciation ratio of HCO_3^- to CO_3^{2-} of 100:1. The surface speciation ratio is a model parameter determined by the expression $\theta = 10^{8.6\text{-}pH}$ as reported by Wolthers et al. (2012). A poor fit is observed between the experimental data and modeled fractionation assuming a surface speciation ratio of HCO_3^- to CO_3^{2-} of 0.25:1. The mismatch, however, is likely explained by a C isotope composition of the surface species DIC that is different than that represented by the bulk solution DIC. Romanek et al. (1992) also varied temperature (10°C, 25°C, and 40°C) during their study and found an average calcite-bicarbonate fractionation of 1.0 ± 0.2‰ for all temperatures. Regardless of rate considerations, the lack of temperature dependence for this study and Romanek et al. (1992) suggests that O isotopes control isotope partitioning between DIC and calcite, and C isotopes have little to no influence. An alternative explanation would be a scenario where there is little to no temperature dependence for the C isotope composition of carbonate ions and calcite primarily forms from CO_3^{2-}.

4.2. Oxygen Isotopes

Calcite from Devils Hole cave system of Nevada, USA, is often invoked to describe equilibrium isotope fractionation due to its very slow rate of precipitation, and this produces a relatively large $^{18}O/^{16}O$ fractionation factor of $10^3\ln(\alpha_{cc\text{-}H_2O}) = 28.09 \pm 0.13$ at ~34°C (Coplen, 2007; Kluge et al., 2014). The error-weighted slope determined in our study is 19.37 in units of $^{18}O/^{16}O$ $10^3\ln\alpha_{cc\text{-}H_2O}$ per 1,000 T^{-1} (K). For comparison, the shaded areas of Figure 3 represent a 95% confidence field between temperature and $10^3\ln(\alpha_{cc\text{-}H_2O})$ as reported by Zaarur et al. (2013) and Kim and O'Neil (1997). These temperature-dependent slopes are 17.8 and 18.0 in units of $^{18}O/^{16}O$ $10^3\ln\alpha_{cc\text{-}H_2O}$ per 1,000 T^{-1} (K) for Zaarur et al. and Kim and O'Neil, respectively. The temperature-dependent equilibrium fractionation derived by Watkins et al. (2013) intersects the proposed fractionation factor for Devils Hole, but is offset to higher $^{18}O/^{16}O$ fractionation than all other experimental studies, including ours (Figure 3). The relations in Figure 3, therefore, most likely reflect a combination of equilibrium and kinetic contributions to the overall O isotope fractionation.

The partitioning of O isotopes during calcite formation from water observed in our experiments is listed in Table 2 and shown in Figure 4 as a function of precipitation rate. The error-weighted slopes for log rate versus $^{18}O/^{16}O$ fractionation at 10°C, 20°C, and 30°C are −0.53 ± 0.40, −1.05 ± 0.35, and −0.62 ± 1.21, respectively, in units of $10^3\ln\alpha_{cc\text{-}H2O}$ per log rate (moles m^{-2} s^{-1}). The 20°C relation might be disproportionately weighted toward a steeper slope due to the faster precipitation rates used in those experiments. These slopes are

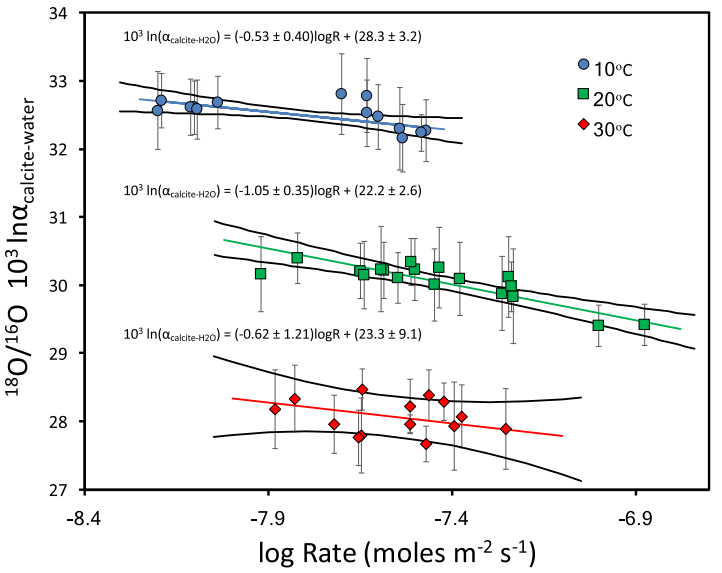

Figure 4. Oxygen isotope fractionation between calcite and water as a function of precipitation rate. Error bars represent propagated 2SD external uncertainty. Error envelopes represent 95% confidence intervals. Equations express error-weighted regressions of the data.

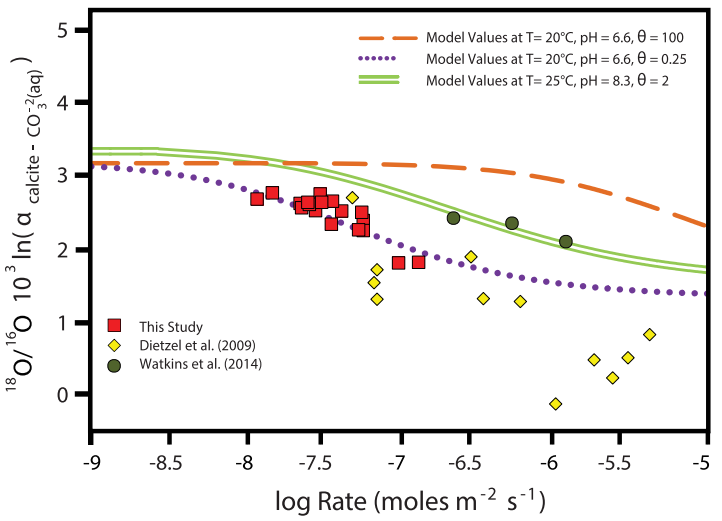

Figure 5. Reproduction of the semiempirical ion-by-ion growth model of Watkins and Hunt (2015) for O isotope fractionation during calcite growth under kinetic and (assumed) equilibrium conditions. The model is based on a "kinetic" regime from the experiments of Watkins et al. (2014, shown by green circle symbols) and inferred equilibrium from Bottinga (1968) and Coplen (2007). The orange dashed line is modeled fractionation for 20°C, *p*H = 6.6, and a surface HCO_3^- to CO_3^{2-} ratio (θ) of 100:1. The purple dotted line is modeled fractionation for 20°C, *p*H = 6.6, and a surface HCO_3^-:CO_3^{2-} ratio (θ) of 0.25:1. Different equilibrium fractionation is predicted for the two different experimental conditions. Also included are values found during this study at 20°C for partitioning between calcite and aqueous carbonate (red squares). Finally, the adjusted (see supporting information text for details) experimental values (T = 20°C, *p*H = 8.3) of Dietzel et al. (2009) are indicated by yellow diamonds.

broadly consistent with analogous slopes of −1.288, −1.279, and −0.624 in units of $^{18}O/^{16}O$ $10^3 \ln\alpha_{cc\text{-}H_2O}$ per log rate (moles m^{-2} s^{-1}) for the 5°C, 25°C, and 40°C syntheses reported by Dietzel et al. (2009). However, a recent study by Devriendt et al. (2017) has asserted that calcite forming from the experiments reported in 2009 was influenced by DIC that was not in equilibrium with solution water. The slightly lower slopes reported here, on the other hand, may be related to the slower precipitation rates, as discussed below, and/or fuller O isotope equilibrium between H_2O and DIC before solid formation.

Oxygen isotope fractionations are a function of precipitation rate (Figure 5), similar to what was found for $^{13}C/^{12}C$ fractionation versus growth rate using the Watkins and Hunt model, but the equivalent trend for $^{18}O/^{16}O$ requires slight modification. The $^{18}O/^{16}O$ fractionation between individual DIC species and calcite inferred by our experiments is lower than those predicted by Watkins and Hunt by up to ~1.5‰ (Figure 5, supporting information Figures S5 and S6). Possible explanations for this observation include (1) the contribution of HCO_3^- and CO_3^{2-} ions on the surface (θ, and to the formation) of solid phase carbonate is not proportional to their concentration ratios in the aqueous phase, (2) invalid use of the Devils' Hole calcite fractionation factor as the assumed equilibrium value as extrapolated to other temperatures, (3) invalid fractionation factors between DIC and water, between individual DIC species, and/or DIC species and calcite, (4) O isotope equilibrium between DIC and water was not actually achieved during the experiments of Watkins et al. (2014), or (5) the fractionation-rate dependence used in the model of Watkins and Hunt (2015) is not valid for *p*H values in the 6–7 range.

We first explore the assumption that HCO_3^- and CO_3^{2-} contribute to calcite in their aqueous proportions as described by the relation $\theta = 10^{8.6\text{-}pH}$. That both species contribute to the O isotope compositions of calcite is suggested by the fact that the measured data plot between the HCO_3^- and CO_3^{2-} isotope compositions. If, however, CO_3^{2-} contributed a greater proportion of O to calcite, the observed data can be fit using a surface HCO_3^-:CO_3^{2-} ratio of 0.25 (Figure 5). Such a change in surface HCO_3^-:CO_3^{2-} ratio, relative to the solution proportion of 100, finds support in the recent study of Andersson et al. (2016), who used density functional theory to show that adsorbed carbonate ions are stable on the surface of calcite even when solutions above the surface-bound ions are characterized by low *p*H (2.4–6.35), where very little CO_3^{2-} exists in solution. The case of low HCO_3^-:CO_3^{2-} speciation is also consistent with the experimentally derived values of Dietzel et al. (2009), who performed a series of experiments at 5°C, 25°C, and 40°C and *p*H between 8.3 and 10.5 (Figure 5, supporting information Figures S5 and S6). In fact, these data were used to help build a new O isotope fractionation model by Devriendt et al. (2017) that operates on the premise that, at equilibrium, $CaCO_3$ forms exclusively from carbonate ions. We have used this model to predict O isotope fractionation between calcite and H_2O based on average conditions measured during our experiments and find excellent agreement (Figure 3) if a small amount of (deprotonated) HCO_3^- is allowed to be incorporated into precipitated calcite. Details and model parameter values are included in supporting information text.

Extrapolation of the Devils Hole results to the conditions of our experiments uses the relation $1,000 \ln(\alpha_{cc\text{-}H_2O}) = 17{,}747/T_K - 29.777$. This

expression was derived to reconcile assumed equilibrium conditions in the Devils Hole system with the kinetic values in the work of Watkins et al. (2013). This temperature dependence is different than observed in this study (Figure 3), which could explain the poor fit between our results and predicted fractionation at 20°C and 30°C, where our regression is most disparate from the Devil's Hole relation (Figure 3). This is supported by the observation that the 10°C experimental data reported here, where our regression is closest to the fractionation expression used by Watkins et al., is more consistent with the predicted model values compared to 20°C and 30°C values (see Figure 5, supporting information Figures S5 and S6).

Although the third and fourth explanations are possible, we consider these unlikely based, in part, on the reproducibility of O isotope fractionation among DIC species described in the work of Beck et al. (2005), Uchikawa and Zeebe (2013), and Tripati et al. (2015). Additionally, biases in the O isotope fractionation factor between any component pair along the path from $CO_{2(aq)}$ to calcite used in the model would need to be lower than the actual equilibrium partitioning. Because the experiments performed here were close to saturation, and hence suspected to closely reflect calcite-water equilibrium, this possibility seems unlikely. The fourth scenario is based on the possibility that the O isotope composition of DIC from which the carbonates precipitated at 25°C in the work of Watkins et al. (2014) was enriched in $^{18}O/^{16}O$ relative to an equilibrium composition. This situation would artificially increase the $\delta^{18}O$ values of the calcite and, accordingly, the calculated $10^3 \ln(\alpha_{cc\text{-}CO_3})$ value (Watkins et al., 2014; Watkins & Hunt, 2015). Watkins et al., however, report that the CO_2(g) used during their experiments was characterized by relatively low $^{18}O/^{16}O$ ratios and would therefore influence the DIC pool toward an anomalously low $\delta^{18}O$ relative to equilibrium with water. This scenario, therefore, seems unlikely.

The final possibility requires that the physical mechanism of calcite growth from solution is different at lower *p*H values, such as, growth at kink sites versus step sites (Morse & Mackenzie, 1990). While this possibility is feasible, actual changes in mechanics during precipitation are impossible to determine from our data. Also, this possibility could be related to differences in accommodating carbonate directly versus indirectly through bicarbonate ions in the calcite lattice upon precipitation. This explanation is supported by an assessment of O isotope fractionation with respect to solution saturation, which suggests that the carbonate formation mechanism may change with increasing supersaturation (see below and supporting information text for further details); this comparison, however, does not control for possible *p*H effects. Nonetheless, collectively, these observations may indicate that the HCO_3^-:CO_3^{2-} ratio incorporated in calcite was distinct from that of the fluid.

Broadly, it is possible that one or more explanations are required to explain the discrepancies observed in Figures 3 and 5. At this time, these are difficult to resolve (and more than one might be true), although HCO_3^-:CO_3^{2-} proportions and uncertainties in the temperature extrapolations of previous studies probably play a role based on the modeling of Watkins et al. Importantly, we have shown that O isotope fractionation appears to be influenced by kinetic factors related to precipitation rate, at least to some degree, in all three temperature series explored. An important conclusion, therefore, is that despite conducting our experiments at very low saturation states, and under conditions where nucleation barriers were removed through the use of seed crystals, it may be difficult to attain complete O isotope equilibrium.

4.3. Clumped Isotopes

A significant body of work now exists that has attempted to reconcile discrepant clumped isotope thermometry calibrations (Dennis & Schrag, 2010; Ghosh et al., 2006; Guo et al., 2009), including the standardization efforts of Dennis et al. (2011). Studies of $^{13}C—^{18}O$ bonding have generally focused on specific carbonates such as deep-sea corals (Thiagarajan et al., 2011), mollusk and brachiopod shells (Henkes, et al., 2013), speleothems (Daeron et al., 2011), and a variety of carbonate compositions studied in experiments, including siderite (Fernandez et al., 2014) and dolomite (Bonifacie et al., 2017; Winkelstern et al., 2016). One goal has been to develop generalized calibrations that are independent of carbonate source (Bonifacie et al., 2017; Deflies et al., 2015; Kelson et al., 2017; Kluge et al., 2015; Murray et al., 2016; Tang et al., 2014; Wacker et al., 2014).

Broadly, the temperature-dependence of $^{13}C—^{18}O$ bonding can be characterized by "high slopes" or "low slopes" on Δ_{47}-temperature diagrams. Recent work has argued that the "high slope" calibration curves are most likely to be correct, including those of Zaarur et al. (2013) and Tripati et al. (2015). In the former two studies, the authors essentially repeated the experiments of Ghosh et al. (2006) and found temperature

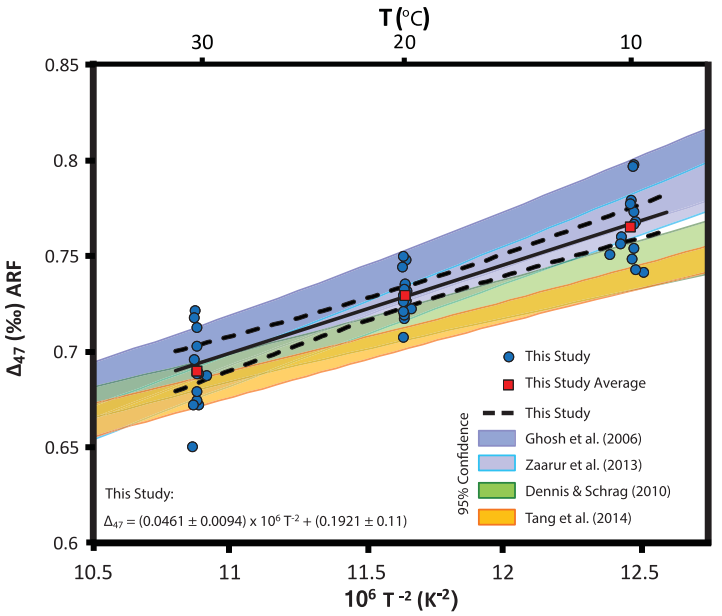

Figure 6. Clumped isotope composition (Δ_{47}) of experimentally precipitated calcite as a function of temperature. For comparison, selected clumped isotope thermometry calibrations are included. The work of Ghosh et al. (2006) and Zaarur et al. (2013) represent "high slope" calibrations, whereas the studies of Dennis and Schrag (2010) and Tang et al. (2014) represent "low slope" calibrations. Error envelope and shaded regions represent 95% confidence intervals for selected studies.

dependent $^{13}C—^{18}O$ bonding very similar to the original clumped isotope thermometry calibration. In the more recent study, $(Ca,Mg)CO_3$ carbonate was investigated and compared to results from $CaCO_3$. Bonifacie et al. (2017) report no difference between Ca-Mg carbonate and Ca carbonate with regard to temperature dependence and $^{13}C—^{18}O$ bonding. They further integrated calibration data from several other studies to put forth a comprehensive calibration expression to cover $(Ca,Mg,Fe)CO_3$ minerals from −1°C to 300°C.

Although the studies described in the previous paragraph provide strong evidence of a single "high slope" Δ_{47}-temperature dependence, different calibrations created from data generated in different analytical systems may, in part, still explain observed offsets between calibrations. The temperature dependence of clumped isotope compositions of carbonates grown in our study, in the absolute reference frame, are compared in Figure 6 with the 95% confidence fields for the calibrations of Ghosh et al. (2006), Dennis and Schrag (2010), and Zaarur et al. (2013), as well as the rate-controlled study of Tang et al. (2014). The average values we measure at 10°C, 20°C, and 30°C agree well with those predicted by Zaarur et al. (2013), supporting the argument that slow precipitation experiments (as opposed to homogeneous nucleation and subsequent heterogeneous carbonate formation) and/or low saturation states promote lattice equilibrium $^{13}C—^{18}O$ bond formation at lower temperatures, where calibrations disagree the most. In general, the temperature-dependence observed for experimental results of this study agree most closely with the "high slope" calibrations over the temperature range explored (Figure 6). For example, the Δ_{47}-temperature dependence found by Zaarur et al. (2013) is described by the equation $\Delta_{47} = (0.0555 \pm 0.0027) \times 10^6\ T^{-2} + (0.0780 \pm 0.0298)$, whereas an error-weighted regression through the data reported here yields $\Delta_{47} = (0.0461 \pm 0.0094) \times 10^6\ T^{-2} + (0.1921 \pm 0.11)$. This regression is also very similar to the combined data calibration reported by Tripati et al. (2015) of $\Delta_{47} = (0.0460 \pm 0.0034) \times 10^6\ T^{-2} + (0.1649 \pm 0.0786)$, as well as the comprehensive calibration of Bonifacie et al. (2017), which is expressed by $\Delta_{47} = (0.0422 \pm 0.0019) \times 10^6\ T^{-2} + (0.1262 \pm 0.0207)$. It should be noted, however, that these similarities may be related to, in part, the fact that our data were generated at Caltech and not on the same equipment as the studies of, for example, Dennis and Schrag (2010) or Tang et al. (2014). On the other hand, however, it should be noted that calcite analyzed by Zaarur et al. was digested in McCrea type vessels at 25°C (rather than a common acid bath at 90°C as in this study), which has been suspected as a possible source of disagreement between various calibrations. Additionally, it should be pointed out that while the saturation states used by Zaarur et al. (2013) have not been reported or estimated, it might be assumed that high saturation states existed if homogeneous nucleation occurred near the start of each experiment. Although we do not feel the different results can be explained completely by differences in laboratories, such issues must be kept in mind.

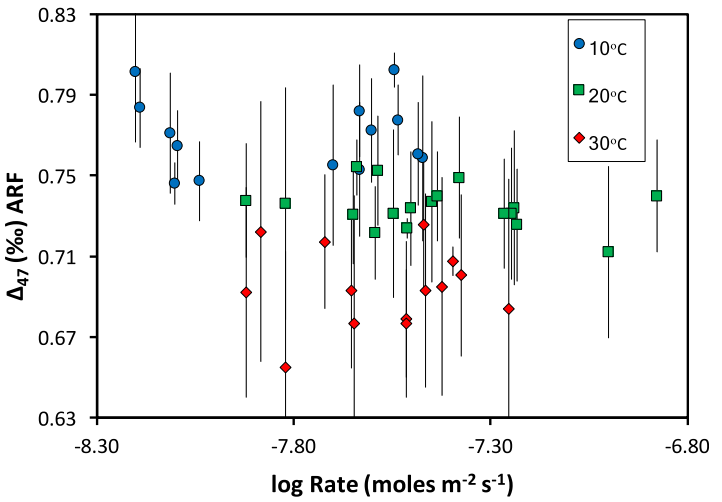

Figure 7. Experimentally determined Δ_{47} for calcite as a function of precipitation rate. Error bars represent propagated 2SD external uncertainty. Error envelopes represent 95% confidence intervals. Equations express error-weighted regressions of the data.

In terms of the experimental approach, the clumped isotope data of this study are most appropriately compared to those of Tang et al. (2014; Dietzel & Usdowski, 1996), who controlled calcite precipitation in the range of 0.02–4.5 μmol m^{-2} s^{-1}, which overlaps the range in our study of 0.006–0.132 μmol m^{-2} s^{-1} (Figure 7 and supporting information Figures S7–S9), although overall the Tang et al. rates are generally higher. It is important to note, however, that Tang et al. did not use seed crystals, and this is an important distinction with our

study, raising the possibility of nucleation effects in their work. Tang et al. (2014) varied *p*H and ionic strengths, in addition to precipitation rates and temperatures. Their *p*H values ranged from 8.3 to 10.5, whereas $CaCl_2$ solution concentrations started at 35 mM and ionic strengths were between 35 to 832 mM. Excluding precipitates from high *p*H solutions ($\geq$10), average Δ_{47} values determined by Tang et al. for precipitated carbonates ranged from 0.754‰ at 5°C to 0.649‰ at 40°C. The authors concluded that *p*H may have an influence on Δ_{47} values at higher *p*H values, but that ionic strength and precipitation rate do not influence clumping under their experimental conditions.

Tripati et al. (2015) present a method for identifying isotope compositions of calcite that are influenced by kinetic fractionation. The study included a series of experiments and quantum chemical calculations to determine the Δ_{63} values for individual DIC species. Specifically, the data and conclusions presented in their work indicate that in addition to bulk O isotope composition of DIC, $^{13}C—^{18}O$ bonding is different among individual DIC species and therefore the clumped isotope composition of total DIC will vary between different *p*H values. Such speciation effects on clumped isotope fractionations are interpreted to be an equilibrium effect in solution but can potentially lead to disequilibrium $^{13}C—^{18}O$ bonding when DIC is incorporated into solid carbonate. The authors put forth an "interfacial model," which describes the possibility of a precipitation rate/regime where C and O isotope reordering at the solution-mineral interface would allow for mineral lattice equilibrium clumping but kinetically influenced incorporation of bulk isotopes according to DIC compositions. This model predicts three contiguous precipitation rate ranges: one which is slow enough to allow mineral lattice equilibrium for $^{13}C—^{18}O$ bonding and direct O isotope equilibrium between calcite and water, a second regime where precipitation is slow enough to allow mineral lattice equilibrium for $^{13}C—^{18}O$ bonding but fast enough to incorporate a kinetic DIC-based fractionation for bulk O isotopes, and a third rapid precipitation range which requires precipitation of carbonate sufficiently quickly that locks in anomalous DIC bulk and clumped isotope compositions in the mineral lattice. Here it should be noted that, regardless of these proposed precipitation regimes, a DIC pool exists in a bulk solution which is independent of mineral surface boundary layer(s). This DIC pool may or may not be in isotopic equilibrium with water. Questions related to how solution DIC influences precipitated calcite isotopes still remain. However, based on the fastest growth conditions of the "interfacial model," Tripati et al. (2015) were also able to show a kinetically controlled Δ_{47}-$\delta^{18}O$ relation that they suggest can be used to evaluate the possibility of the third type of (kinetically controlled) fractionation in carbonates. This relation has been evaluated for the data reported here, and we find no correlation between Δ_{47} and $10^3\ln(\alpha_{calcite-H_2O})$ (supporting information Figure S10).

The treatment of clumped isotopes in the model of Watkins and Hunt (2015) is heavily based on an equilibrium Δ_{63} value of the Devil's Hole calcite and the temperature-dependent $^{13}C—^{18}O$ bonding determined for calcite, HCO_3^-, and CO_3^{2-} by Hill et al. (2014). However, calculated $^{13}C—^{18}O$ bonding for DIC species may be underestimated based on a comparison between experimental calcite work and the Δ_{63}-T relation determined by Hill et al (2014). The model predicts an approximately $+0.005‰$ difference between equilibrium $^{13}C—^{18}O$ bonding and the (higher frequency) bonding calculated at our precipitation rates (supporting information Figures S7–S9). Offsets at this level are not detectable by conventional analytical methods, although, the direction of the offset is worth considering. The positive shift (higher Δ_{63} value) predicted at faster precipitation rates from solutions with *p*H lower than ~10 is related to the HCO_3^-:CO_3^{2-} ratio in solution and the higher clumped isotope composition of HCO_3^- compared to CO_3^{2-} (Hill et al., 2014; Tripati et al., 2015). In other words, the model predicts that quickly forming calcite will inherit the species-weighted average of DIC $^{13}C—^{18}O$ bonding, and therefore disequilibrium calcite can record a higher Δ_{63} value because aqueous HCO_3^- at equilibrium has a higher Δ_{63} value than equilibrium calcite at the same temperature. This scenario is opposite of the effect expected when saturation state (and by extension, precipitation rate) is increased by raising *p*H. Under these conditions, solution DIC composition shifts to a lower HCO_3^-:CO_3^{2-} ratio causing the composite Δ_{63} to decrease. Above a *p*H of approximately 10, rapid precipitation would cause a negative offset in calcite Δ_{63} according to the model of Watkins and Hunt (2015).

Saturation state is a first-order factor controlling carbonate precipitation rate. The experimental conditions utilized during our study do not include a wide enough range of saturation states to investigate a correlation between degree of saturation and $^{13}C—^{18}O$ bonding, although the wider range in saturation state of previous studies allow evaluation of this parameter. Calcite precipitation mechanisms and rate laws are thought to change as a function of saturation states, but, within a given saturation state, factors such as *p*H,

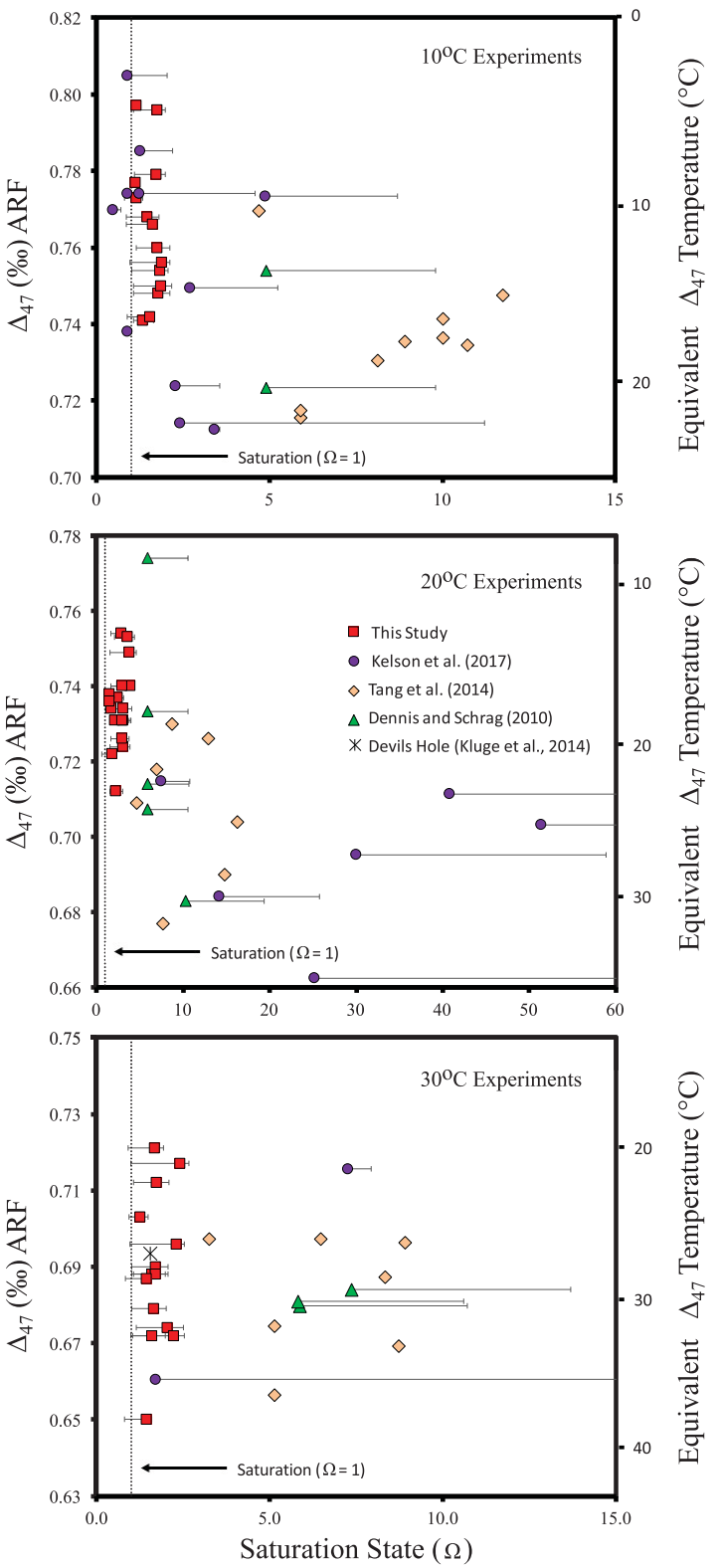

ionic strength, reagent ion ratios, or substrate morphology are also important (Hong & Teng, 2014; Sand et al., 2016; Teng et al., 2000; van der Weijden & van der Weijden, 2014).

In comparing our results to previous studies, several adjustments must be made to align different studies as closely as possible. Experimentally determined Δ_{47} values from Dennis and Schrag (2010), Tang et al. (2014), and Kelson et al. (2017) have been projected to precipitation temperatures of 10°C, 20°C, or 30°C for direct comparison to the results of this study (Figure 8). Additionally, the Devils Hole calcite ($\Omega = 1.5 \pm 0.09$) may also be considered. Individual experimental values from previous work in the range of 0–14°C, 15–24°C, and 25–40°C have been converted to 10°C, 20°C, and 30°C, respectively, and these adjustments have been made according to the Δ_{47}-T relations determined in each respective study, retaining data set variability for each set of conditions (see supporting information text for full details). The following comparison is only qualitative because the experiments conducted by Dennis and Schrag (2010) and Kelson et al. (2017) were characterized by decreasing saturation state over the course of precipitation, whereas the Tang et al. (2014) experiments likely utilized higher saturation state during carbonate formation initiation by homogeneous nucleation.

An apparent correlation of increasing Δ_{47} values with decreasing saturation state can be seen in the collective data sets at lower temperatures (Figure 8). This correlation is most prominent at temperatures between 0°C and 14°C, less pronounced between 15°C and 24°C, and absent above 24°C. These observations indicate that saturation state is an important factor controlling $^{13}C—^{18}O$ bonding during calcite formation from solution at lower temperatures where calibrations show maximum divergence. Such relations may be explained in two ways. First, they may indicate that precipitation mechanism may be more sensitive to different saturation states at lower temperatures. Second, the rate of $^{13}C—^{18}O$ bond reordering at the solution-mineral interface in the interfacial model of Tripati et al. (2015) may be slower at lower temperatures given similar saturation conditions. In other words, at a given medium to high saturation state, $^{13}C—^{18}O$ bond reordering at the solution-mineral interface may achieve equilibrium at higher temperatures where reordering kinetics are possibly faster but from the

Figure 8. Comparison of experimentally determined Δ_{47} for calcite from multiple studies as a function of solution saturation state with respect to calcite. All experimental values represent average conditions for a given experimental run and have been adjusted to represent $^{13}C—^{18}O$ bonding at 10°C, 20°C, and 30°C (see supporting information text for adjustment description). Error bars for data points from this study represent maximum and minimum saturation based on measured solution conditions. Error bars for the data points of Kelson et al. (2017) and Dennis and Schrag (2010) represent maximum saturation based on reported solution conditions or saturation states. In cases where both starting and ending master solution conditions were not reported, a minimum (end of experiment) saturation state of $\Omega = 1$ was assumed. The saturation states of Tang et al. (2014) were used as reported in Tang et al. (2008). The vertical dotted lines represent saturation (equilibrium, $\Omega = 1$). The temperatures indicated on the second (right side) vertical axes illustrate the equivalent temperatures as the range in Δ_{47} values reflect, and are based on the clumped isotope calibration of Zaarur et al. (2013).

same solution at lower temperatures, calcite may not achieve equilibrium $^{13}C—^{18}O$ bonding where reordering kinetics appear to be slower.

5. Conclusions

Recent developments in the understanding of H_2O-CO_2-carbonate system equilibrium and isotope fractionations associated with carbonate precipitation reactions requires a critical reassessment of $^{13}C—^{18}O$ bond formation in carbonates and their relations to the DIC system. We have used the chemo-stat synthetic precipitation method to produce slowly growing calcite under slightly supersaturated conditions to explore the relation between formation rate and C and O isotope fractionation as well as clumped isotope fractionation. The log precipitation rates explored during this study ranged from -6.88 to -8.20 mol m^{-2} s^{-1}, among the slowest precipitation rates obtained in experiments on isotopic fractionation in carbonates. In addition, the use of isotopically labeled seed crystals allowed minimization of kinetic effects that may be produced during mixed precipitation mechanisms during homogeneous nucleation followed by heterogeneous crystal growth. As a result, very low saturation states characterized the experiments, less than four times equilibrium.

We found C isotope fractionation between calcite and bicarbonate ions to exhibit nontemperature-dependent partitioning of approximately $1.6 \pm 0.4‰$ between 10°C and 30°C. In contrast, O isotope fractionation between calcite and water was observed to exhibit temperature-dependent isotopic fractionation, but only minor rate-dependent isotopic fractionation over the range of conditions of the experiments. $^{18}O/^{16}O$ fractionation was found to be higher than those measured in many previous experiments, with a temperature relation of $10^3 \ln(\alpha_{calcite-H_2O}) = (19.27 \pm 0.68) \times 10^3\ T^{-1} + (-35.60 \pm 0.4)$. Isotopic fractionation for calcite $^{13}C—^{18}O$ bonding, expressed as Δ_{47}, was also observed to be rate independent over the conditions explored. As expected, formation temperature played a major role in carbonate clumped isotope compositions and we obtained the following relation: $\Delta_{47} = (0.0461 \pm 0.0094) \times 10^6\ T^{-2} + (0.1921 \pm 0.11)$.

Although our experimental approach was intended to closely approach equilibrium conditions, it is possible, even likely, that kinetic isotope effects remain. We find an average C isotope fractionation that is higher than the study of Romanek et al. (1992) but lower than those of Bottinga (1968) and Coplen (2007). Our C isotope results closely follow the ion-by-ion growth model of Watkins and Hunt (2015). Our results for O isotope fractionation, however, do not fully support the Watkins and Hunt model unless some significant modifications are made, including treatment of surface DIC speciation, among other factors. Although the rate dependence for O isotope fractionations trend similarly to model predictions, the magnitude of partitioning between calcite and DIC suggests that calcite formed from a surface that disproportionately sequestered carbonate ions instead of bicarbonate ions onto calcite surfaces in our experiments. This mechanism of carbonate formation may be related to saturation state, which has been shown to have a negative correlation with $^{13}C—^{18}O$ bonding, as well as possibly $^{18}O/^{16}O$ fractionations at lower temperatures. If this conclusion is true, this suggests that equilibrium $^{18}O/^{16}O$ fractionation between calcite and water is higher than commonly believed. This study adds to the growing body of evidence which suggests that O isotope thermometry calibrations including, or at least more similar in magnitude to, the $^{18}O/^{16}O$ fractionation indicated by Devils Hole calcite (Coplen, 2007; Kluge et al., 2014), are preferable to previous experimental studies. Finally, clumped isotope data presented here supports the "higher" slope calibration of Zaarur et al. (2013) over the temperature range explored. This study also supports the "interfacial" calcite formation model presented by Tripati et al. (2015), whereby certain precipitation rate regimes can decouple bulk isotope fractionation and clumped isotope bonding frequency in a mineral lattice.

Acknowledgments
Nami Kitchen is recognized for instrument and analytical assistance. The Stable Isotope Facility at UC-Davis is appreciated for supporting analyses. We thank James M. Watkins, Hagit P. Affek, and three anonymous reviewers for helpful comments and suggestions that greatly improved this document. We also thank Aradhna E. Tripati for her editorial handling. This work was supported by the NASA Headquarters under the NASA Earth and Space Science Fellowship Program—grant NNX13AP40H as well as NASA Astrobiology Institute grant NNA13AA94A. The authors declare no conflicts of interest from their affiliation or funding.

References

Affek, H. P. (2013). Clumped isotope equilibrium and the rate of isotope exchange between CO_2 and water. *American Journal of Science*, *313*, 309–325.

Affek, H. P., Bar-Matthews, M., Ayalon, A., Matthews, A., & Eiler, J. M. (2008). Glacial/interglacial temperature variations in Soreq cave speleothems as recorded by 'clumped isotope' thermometry. *Geochimica et Cosmochimica Acta*, *72*, 5351–5360.

Affek, H. P., & Eiler, J. M. (2006). Abundance of mass 47 CO_2 in urban air, car exhaust, and human breath. *Geochimica et Cosmochimica Acta*, *70*, 1–12.

Affek, H. P., Matthews, A., Ayalon, A., Bar-Matthews, M., Burstyn, Y., Zaarur, S., et al. (2014). Accounting for kinetic isotope effects in Soreq Cave (Israel) speleothems. *Geochimica et Cosmochimica Acta*, *143*, 303–318.

Affek, H. P., & Zaarur, S. (2014). Kinetic isotope effect in CO_2 degassing: Insights from clumped and oxygen isotopes in laboratory precipitation experiments. *Geochimica et Cosmochimica Acta*, *143*, 319–330.
Albarède, F., & Beard, B. L. (2004). Analytical methods for non-traditional isotopes. *Reviews in Mineralogy and Geochemistry*, *55*, 113–152.
Andersson, M. P., Rodriguez-Blanco, J. D., & Stipp, S. L. S. (2016). Is bicarbonate stable in and on the calcite surface? *Geochimica et Cosmochimica Acta*, *176*, 198–205.
Beck, W. C., Grossman, E. L., & Morse, J. W. (2005). Experimental studies of oxygen isotope fractionation in the carbonic acid system at 15°, 25°, and 40°C. *Geochimica et Cosmochimica Acta*, *69*(14), 3493–3503.
Bonifacie, M., Calmels, D., Eiler, J. M., Horita, J., Chaduteau, C., Vasconcelos, C., et al. (2017). Calibration of the dolomite clumped isotope thermometer from 25 to 350°C, and implications for a universal calibration for all (Ca,Mg,Fe)CO_3 carbonates. *Geochimica et Cosmochimica Acta*, *200*, 255–279.
Bottinga, Y. (1968). Calculation of fractionation factors for carbon and oxygen isotopic exchange in the system calcite-carbon dioxide-water. *Journal of Physical Chemistry*, *72*(3), 800–808.
Brand, W. A., Assonov, S. S., & Coplen, T. B. (2010). Correction for the ^{17}O interference in $\delta^{13}C$ measurements when analyzing CO_2 with stable isotope mass spectrometry (IUPAC technical report). *Pure and Applied Chemistry*, *82*, 1719–1733.
Brunauer, S., Emmett, P., & Teller, E. (1938). Adsorption of gases in multimolecular layers. *Journal of the American Chemical Society*, *60*, 309–319.
Came, R. E., Brand, U., & Affek, H. P. (2014). Clumped isotope signatures in modern brachiopod carbonate. *Chemical Geology*, *377*, 20–30.
Came, R. E., Eiler, J. M., Veizer, J., Azmy, K., Brand, U., & Weidman, C. R. (2007). Coupling of surface temperatures and atmospheric CO_2 concentrations during the Palaeozoic era. *Nature*, *449*, 198–201.
Coplen, T. (2007). Calibration of the calcite-water oxygen-isotope geothermometer at Devils Hole, Nevada, a natural laboratory. *Geochimica et Cosmochimica Acta*, *71*(16), 3948–3957.
Cummins, R. C., Finnegan, S., Fike, D. A., Eiler, J. M., & Fischer, W. W. (2014). Carbonate clumped isotope constraints on Silurian ocean temperature and seawater $\delta^{18}O$. *Geochimica et Cosmochimica Acta*, *140*, 241–258.
Daeron, M., Blamart, D., Peral, M., & Affek, H. P. (2016). Absolute isotopic abundance ratios and the accuracy of Δ_{47} measurements. *Chemical Geology*, *442*, 83–96.
Daeron, M., Guo, W., Eiler, J. M., Genty, D., Blamart, D., Boch, R., et al. (2011). $^{13}C^{18}O$ clumping in speleothems: Observations from natural caves and precipitation experiments. *Geochimica et Cosmochimica Acta*, *75*, 3303–3317.
Deflies, W. F., Hren, M. T., & Lohmann, K. C. (2015). Compositional and temperature effects of phosphoric acid fractionation on δ_{47} analysis and implications for discrepant calibrations. *Chemical Geology*, *396*, 51–60.
Dennis, K. J., Affek, H. P., Passey, B. P., Schrag, D. P., & Eiler, J. M. (2011). Defining an absolute reference frame for 'clumped' isotope studies of CO_2. *Geochimica et Cosmochimica Acta*, *75*(22), 7117–7131.
Dennis, K. J., & Schrag, D. P. (2010). Clumped isotope thermometry of carbonatites as an indicator of diagenetic alteration. *Geochimica et Cosmochimica Acta*, *74*(14), 4110–4122.
Devriendt, L. S., Watkins, J. M., & McGregor, H. V. (2017). Oxygen isotope fractionation in the $CaCO_3$-DIC-H_2O system. *Geochimica et Cosmochimica Acta*, *214*, 115–142.
Dietzel, M., Tang, J., Leis, A., & Kohler, S. J. (2009). Oxygen isotopic fractionation during inorganic calcite precipitation—Effects of temperature, precipitation rate and pH. *Chemical Geology*, *268*, 107–115.
Dietzel, M., & Usdowski, E. (1996). Coprecipitation of Ni^{2+}, Co^{2+}, and Mn^{2+} with galena and covellite, and of Sr^{2+} with calcite during crystallization via diffusion of H_2S and CO_2 through polyethylene at 20°C: Power law and Nernst law control of trace element partitioning. *Chemical Geology*, *131*(1–4), 55–65.
Eagle, R. A., Eiler, J. M., Tripati, A. K., Ries, J. B., Freitas, P. S., Hiebenthal, C., et al. (2013). The influence of temperature and seawater carbonate saturation state on $^{13}C—^{18}O$ bond ordering in bivalve mollusks. *Biogeosciences*, *10*, 4591–4606.
Eiler, J. M. (2007). Clumped-isotope" geochemistry—The study of naturally-occurring, multiply-substituted isotopologues. *Earth and Planetary Science Letters*, *262*(3–4), 309.
Eiler, J. M. (2011). Paleoclimate reconstruction using carbonate clump isotope thermometry. *Quaternary Science Reviews*, *30*, 3575–3588.
Epstein, S., Buchsbaum, R., Lowenstam, H. A., & Urey, H. C. (1953). Revised carbonate-water isotopic temperature scale. *Geological Society of America Bulletin*, *64*, 1315–1326.
Faure, G., & Mensing, T. M. (2009). *Isotopes principles and applications* (3rd ed.). New York, NY: John Wiley & Sons, Inc.
Fernandez, A., Tang, J., & Rosenheim, B. (2014). Siderite "clumped" isotope thermometry: A new paleoclimate proxy for humid continental environments. *Geochimica et Cosmochimica Acta*, *126*, 411–421.
Finnegan, S., Bergmann, K., Eiler, J. M., Jones, D. S., Fike, D. A., Eisenman, I., et al. (2011). The magnitude and duration of late Ordovician-early Silurian glaciation. *Science*, *331*, 903–906.
Gabitov, R. I., Watson, E. B., & Sadekov, A. (2012). Oxygen isotope fractionation between calcite and fluid as a function of growth rate and temperature: An in situ study. *Chemical Geology*, *306–307*, 92–102.
Gagnon, A. C., DePaolo, D. J., & Adkins, J. F. (2012). Precise overgrowth composition during biomineral culture and inorganic precipitation. *Chemical Geology*, *330–331*, 188–196.
Ghosh, P., Adkins, J., Affek, H. P., Balta, B., Guo, W. F., Schauble, E. A., et al. (2006). $^{13}C—^{18}O$ bonds in carbonate minerals: A new kind of paleothermometer. *Geochimica et Cosmochimica Acta*, *70*(6), 1439–1456.
Guo, W. F. (2008). *Carbonate clumped isotope thermometry: Application to carbonaceous chondrites and effects of kinetic isotope fractionation* (PhD thesis). Pasadena, CA: Division of Geology and Planetary Science, Caltech.
Guo, W. F., Mosenfelder, J., Goddard, W., & Eiler, J. M. (2009). Isotopic fractionations associated with phosphoric acid digestion of carbonate minerals: Insights from first-principles theoretical modeling and clumped isotope measurements. *Geochimica et Cosmochimica Acta*, *73*(24), 7203.
Henkes, G. A., Passey, B. H., Wanamaker, A. D., Grossman, E. L., Ambrose, W. G., & Carroll, M. L. (2013). Carbonate clumped isotope compositions of modern marine mollusk and brachiopod shells. *Geochimica et Cosmochimica Acta*, *106*, 307–325.
Hill, P. S., Tripati, A. K., & Schauble, E. A. (2014). Theoretical constraints on the effects of pH, salinity, and temperature on clumped isotope signatures of dissolved inorganic carbon species and precipitating carbonate minerals. *Geochimica et Cosmochimica Acta*, *125*, 610–652.
Hong, M., & Teng, H. H. (2014). Implications of solution chemistry effects: Direction-specific restraints on the step kinetics of calcite growth. *Geochimica et Cosmochimica Acta*, *141*, 228–239.
Huntington, K. W., Eiler, J. M., Affek, H. P., Guo, W., Bonifacie, M., Yeung, L. Y., et al. (2009). Methods and limitations of 'clumped' CO_2 isotope (Δ_{47}) analysis by gas-source isotope ratio mass spectrometry. *Journal of Mass Spectrometry*, *44*(9), 1318–1329.
Jimenez-Lopez, C., & Romanek, C. S. (2004). Precipitation kinetics and carbon isotope partitioning of inorganic siderite at 25 degrees C and 1 atm. *Geochimica et Cosmochimica Acta*, *68*(3), 557–571.

Kelson, J. R., Huntington, K. W., Schauer, A. J., Saenger, C., & Lechler, A. R. (2017). Toward a universal carbonate clumped isotope calibration: Diverse synthesis and preparatory methods suggest a single temperature relationship. *Geochimica et Cosmochimica Acta*, *197*, 104–131.

Kim, S.-T., & O''Neil, J. R. (1997). Equilibrium and nonequilibrium oxygen isotope effects in synthetic carbonates. *Geochimica et Cosmochimica Acta*, *61*(16), 3461.

Kluge, T., & Affek, H. P. (2012). Quantifying kinetic fractionation in Bunker Cave speleothems using Δ_{47}. *Quaternary Science Reviews*, *49*, 82–94.

Kluge, T., Affek, H. P., Dublyansky, Y., & Spötl, C. (2014). Devils Hole paleotemperatures and implications for oxygen isotope equilibrium fractionation. *Earth and Planetary Science Letters*, *400*, 251–260.

Kluge, T., Affek, H. P., Marx, T., Aeschbach-Hertig, W., Riechelmann, D. F. C., Scholz, D., et al. (2013). Reconstruction of drip-water $\delta^{13}C$ based on calcite and clumped isotopes from Bunker Cave (Germany). *Climate of the Past*, *9*, 377–391.

Kluge, T., John, C. M., Jourdan, A. L., Davis, S., & Crawshaw, J. (2015). Laboratory calibration of the calcium carbonate clumped isotope thermometer in the 25–250°C temperature range. *Geochimica et Cosmochimica Acta*, *157*, 213–227.

Levitt, N. P., & Romanek, C. S. (2016). An ''on-line'' method for oxygen isotope exchange between gas phase CO_2 and water. *Aquatic Geochemistry*, *22*, 253–269.

Li, W., Chakraborty, S., Beard, B. L., Romanek, C. S., & Johnson, C. M. (2012). Magnesium isotope fractionation during precipitation of inorganic calcite under laboratory conditions. *Earth and Planetary Science Letters*, *333–334*, 304–316.

McCrea, J. M. (1950). On the isotopic chemistry of carbonates and a paleotemperature scale. *Journal of Chemical Physics*, *18*, 849–857.

Mills, G. A., & Urey, H. C. (1940). The kinetics of isotopic exchange between carbon dioxide, bicarbonate ion, carbonate ion and water. *Journal of the American Chemical Society*, *62*, 1019–1026.

Morse, J. W. (1974). Dissolution kinetics of calcium carbonate in sea water. III. A new method for the study of carbonate reaction kinetics. *American Journal of Science*, *274*, 97–107.

Morse, J. W., & Mackenzie, F. T. (1990). *Geochemistry of sedimentary carbonates*. New York, NY: Elsevier Science Publishers Inc.

Mucci, A., & Morse, J. W. (1983). The incorporation of Mg^{2+} and Sr^{2+} into calcite overgrowths: Influences of growth rate and solution composition. *Geochimica et Cosmochimica Acta*, *47*, 2 17–233.

Murray, S. T., Arienzo, M. M., & Swart, P. K. (2016). Determining the Δ_{47} acid fractionation in dolomites. *Geochimica et Cosmochimica Acta*, *174*, 42–53.

Ogino, T., Suzuki, T., & Sawada, K. (1987). The formation and transformation mechanism of calcium carbonate in water. *Geochimica et Cosmochimica Acta*, *51*, 2757–2767.

Olack, G., & Coleman, A. (2016). *Influence of ^{17}O correction parameters on calculation and calibration of Δ_{47}*. Abstract presented at Goldschmidt Conference Yokohama, Japan 26 June–1 July, 2016 (p. 2378).

O'Neil, J. R., & Adami, L. H. (1969). Oxygen isotope partition function ratio of water and the structure of liquid water. *Journal of Physical Chemistry*, *73*(5), 1553–1558.

Parkhurst, D. L., & Appelo, C. A. J. (2013). Description of input and examples for PHREEQC version 3—A computer program for speciation, batch-reaction, one-dimensional transport, and inverse geochemical calculations. In *U.S. Geological Survey techniques and methods* (book 6, Chapter A43, 497 p.). Reston, VA: U.S. Geological Survey. Retrieved from http://pubs.usgs.gov/tm/06/a43/.

Passey, B. H., Levin, N. E., Cerling, T. E., Brown, F. H., & Eiler, J. M. (2010). High-temperature environments of human evolution in East Africa based on bond ordering in paleosol carbonates. *Proceedings of the National Academy of Sciences of the United States of America*, *107*, 11245–11249.

Petryshyn, V. A., Lim, D., Laval, B. L., Brady, A., Slater, G., & Tripati, A. K. (2015). Reconstruction of limnology and microbialite formation conditions from carbonate clumped isotope thermometry. *Geobiology*, *13*, 53–67.

Rodriguez-Blanco, J. D., Shaw, S., & Benning, L. G. (2011). The kinetics and mechanisms of amorphous calcium carbonate (ACC) crystallization to calcite, via vaterite. *Nanoscale*, *3*, 265–271.

Romanek, C. S., Grossman, E. L., & Morse, J. W. (1992). Carbon isotopic fractionation in synthetic aragonite and calcite—Effects of temperature and precipitation rate. *Geochimica et Cosmochimica Acta*, *56*(1), 419–430.

Romanek, C. S., Morse, J. W., & Grossman, E. L. (2011). Aragonite kinetics in dilute solutions. *Aquatic Geochemistry*, *17*(4–5), 339–356.

Sade, Z., & Halevy, I. (2017). New constraints on kinetic isotope effects during CO_2(aq) hydration and hydroxylation: Revisiting theoretical and experimental data. *Geochimica et Cosmochimica Acta*, *214*, 246–265.

Saenger, C., Affek, H. P., Felis, T., Thiagarajan, N., Lough, J. M., & Holcomb, M. (2012). Carbonate clumped isotope variability in shallow water corals: Temperature dependence and growth-related vital effects. *Geochimica et Cosmochimica Acta*, *99*, 224–242.

Sand, K. K., Tobler, D. J., Dobberschutz, S., Larsen, K. K., Makovicky, E., Andersson, M. P., et al. (2016). Calcite growth kinetics: Dependence on saturation index, Ca^{2+}:CO_3^{2-} activity ratio, and surface atomic structure. *Crystal Growth & Design*, *16*, 3602–3612.

Santrock, J., Studley, S. A., & Hayes, J. M. (1985). Isotopic analyses based on the mass spectrum of carbon dioxide. *Analytical Chemistry*, *57*(7), 1444–1448.

Schauble, E. A., Ghosh, P., & Eiler, J. M. (2006). Preferential formation of ^{13}C—^{18}O bonds in carbonate minerals, estimated using first principles lattice dynamics. *Geochimica et Cosmochimica Acta*, *70*, 2510–2529.

Schauer, A. J., Kelson, J., Saenger, C., & Huntington, K. W. (2016). Choice of ^{17}O correction affects clumped isotope (Δ_{47}) values of CO_2 measured with mass spectrometry. *Rapid Communications in Mass Spectrometry*, *30*, 2607–2616.

Spooner, P. T., Guo, W., Robinson, L. F., Thiagarajan, N., Hendry, K. R., Rosenheim, B. E., & Leng, M. J. (2016). Clumped isotope composition of cold-water corals: A role for vital effects? *Geochimica Cosmochimica Acta*, *179*, 123–141.

Swart, P. K., Burns, S. J., & Leder, J. J. (1991). Fractionation of the stable isotopes of oxygen and carbon in carbon dioxide during the reaction of calcite with phosphoric acid as a function of temperature and technique. *Chemical Geology: Isotope Geoscience Section*, *86*(2), 89–96.

Tang, J., Dietzel, M., Fernandez, A., Tripati, A. K., & Rosenheim, B. E. (2014). Evaluation of kinetic effects on clumped isotope fractionation (Δ_{47}) during inorganic calcite precipitation. *Geochimica et Cosmochimica Acta*, *134*, 120–136.

Tang, J., Köhler, S., & Dietzel, M. (2008). Sr^{2+}/Ca^{2+} and $^{44}Ca/^{40}Ca$ fractionation during inorganic calcite formation: I. Sr incorporation. *Geochimica et Cosmochimica Acta*, *72*(15), 3718–3745.

Teng, H. H., Dove, P. M., & Yoreo, J. J. (2000). Kinetics of calcite growth: Surface processes and relationships to macroscopic rate laws. *Geochimica et Cosmochimica Acta*, *64*(13), 2255–2266.

Thiagarajan, N., Adkins, J., & Eiler, J. M. (2011). Carbonate clumped isotope thermometry of deep sea corals and implications for vital effects. *Geochimica et Cosmochimica Acta*, *75*, 4416–4425.

Tripati, A. K., Eagle, R. A., Thiagarajan, N., Gagnon, A. C., Bauch, H., Halloran, P. R., et al. (2010). ^{13}C—^{18}O isotope signatures and ''clumped isotope'' thermometry in foraminifera and coccoliths. *Geochimica et Cosmochimica Acta*, *74*, 5697–5717.

Tripati, A. K., Hill, P. S., Eagle, R. A., Mosenfelder, J. L., Tang, J., Schauble, E. A., et al. (2015). Beyond temperature: Clumped isotope signatures in dissolved inorganic carbon species and the influence of solution chemistry on carbonate mineral composition. *Geochimica et Cosmochimica Acta*, *166*, 344–371.

Uchikawa, J., & Zeebe, R. E. (2012). The effect of carbonic anhydrase on the kinetics and equilibrium of the oxygen isotope exchange in the CO_2-H_2O system: Implications for delta —^{18}O vital effects in biogenic carbonates. *Geochimica et Cosmochimica Acta*, *95*, 15–34.

Uchikawa, J., & Zeebe, R. E. (2013). No discernible effect of Mg^{2+} ions on the equilibrium oxygen isotope fractionation in the CO_2-H_2O system. *Chemical Geology*, *343*, 1–11.

Urey, H. C. (1947). The thermodynamic properties of isotopic substances. *Journal of the Chemical Society*, May, 562–581.

Van der Weijden, C. H., & van der Weijden, R. D. (2014). Calcite growth: Rate dependence on saturation, on ratios of dissolved calcium and (bi)carbonate and on their complexes. *Journal of Crystal Growth*, *394*, 137–144.

Wacker, U., Fiebig, J., Tödter, J., Schöne, B., Bahr, A., Friedrich, O., et al. (2014). Empirical calibration of the clumped isotope paleothermometer using calcites of various origins. *Geochimica et Cosmochimica Acta*, *141*, 127.

Wang, Z. G., Schauble, E. A., & Eiler, J. M. (2004). Equilibrium thermodynamics of multiply substituted isotopologues of molecular gases. *Geochimica et Cosmochimica Acta*, *68*(23), 4779–4797.

Watkins, J. M., & Hunt, J. D. (2015). A process-based model for non-equilibrium clumped isotope effects in carbonates. *Earth and Planetary Science Reviews*, *432*, 152–165.

Watkins, J. M., Hunt, J. D., Ryerson, F. J., & DePaolo, D. J. (2014). The influence of temperature, pH, and growth rate on the $\delta^{18}O$ composition of inorganically precipitated calcite. *Earth and Planetary Science Reviews*, *404*, 332–343.

Watkins, J. M., Nielsen, L. C., Ryerson, F. J., & DePaolo, D. J. (2013). The influence of kinetics on the oxygen isotope composition of calcium carbonate. *Earth and Planetary Science Letters*, *375*, 349–360.

Winkelstern, I. Z., Kaczmarek, S. E., Lohmann, K. C., & Humphrey, J. D. (2016). Calibration of dolomite clumped isotope thermometry. *Chemical Geology*, *443*, 32–38.

Wolthers, M., Nehrke, G., Gustafsson, J. P., & Cappellen, P. V. (2012). Calcite growth kinetics: Modeling the effect of solution stoichiometry. *Geochimica et Cosmochimica Acta*, *77*, 121–134.

Zaarur, S., Affek, H. P., & Brandon, M. T. (2013). A revised calibration of the clumped isotope thermometer. *Earth and Planetary Science Reviews*, *382*, 47–57.

Zeebe, R. E. (2014). Kinetic fractionation of carbon and oxygen isotopes during hydration of carbon dioxide. *Geochimica et Cosmochimica Acta*, *139*, 540–552.

Zeebe, R. E., & Wolf-Gladrow, D. (2001). *CO_2 in seawater: Equilibrium, kinetics, isotopes*. Amsterdam, Netherlands: Elsevier Science B.V. (Oceanography Series).

Erratum

In the originally published version of this article, in the numerator of Equation 5, the multiplication symbol was incorrectly set as an addition symbol. The equation has since been corrected, and this version may be considered the authoritative version of record.